



Manufacture and investigation on the shape memory polymer composite subsidy pipe



Zhaokun Ren^a, Yulai Sun^b, Qiongwei Li^b, Lihua Yang^b, Liwu Liu^{a,*}, Yanju Liu^a, Jinsong Leng^{c,*}

^a Department of Astronautical Science and Mechanics, Harbin Institute of Technology (HIT), P.O.Box 301, No.92 West Dazhi Street, Harbin 150001, People's Republic of China

^b Oil & Gas Technology Research Institute, Changqing Oilfield Branch Company, Petrochina, Xi'an 710018, China

^c Centre for Composite Materials and Structures, Harbin Institute of Technology (HIT), Harbin 150080, People's Republic of China

ARTICLE INFO

Keywords:

SMPC
Pipe
Subsidy
Failure

ABSTRACT

In this paper, a process for restoring damaged pipelines based on shape memory polymer composites (SMPC) was introduced, and the corrosion resistance and mechanical properties of SMPC were evaluated. First and foremost, SMPC was used for repairing damaged oil pipelines. Referring to the wet winding method, the subsidy pipe based on SMPC was fabricated by winding in the axial direction of $\pm 45^\circ$. According to the failure theory of composite material, the minimum wall thickness of the subsidy pipe to withstand the pressure was determined. The effects of fiber content and temperature on the structural stiffness of semi-circular hinges with different ratios of carbon fiber were observed. Radial and axial compression tests were carried out on the subsidy pipe to study the effect of compression times and temperature on the stiffness. Radial compression tests are conducted on the subsidy pipes with different wall thicknesses to determine the effect of wall thickness on the stiffness.

1. Introduction

Shape memory polymer composite (SMPC) has been extensively used in the field of aerospace due to its advantages such as high specific stiffness and strength and strong capability of generating memory effect by sensing external excitation [1–5]. Lots of scholars have proposed related thermodynamic constitutive equations and studied the corresponding mechanical behavior on SMP and SMPC, which can be used to describe the shape memory effect. Tobushi first proposed a nonlinear thermodynamic behavior model to explain the shape memory effect using polyurethane as the research object [6,7]. Liu created the phase transition theory, scilicet, SMP is mainly composed of Frozen Phase and Active Phase, as the external temperature changes, the volume fraction of the two phases makes an alternation continuously, in the meantime, it is assumed that the strain generated by the SMP at high temperature is frozen and stored while the temperature is lower, as the ambient temperature rises, the original frozen strain is released again [8]. In addition to studying the thermodynamic constitutive model of pure SMP, Tan et al. investigated the constitutive model of SMPC, namely, the material is composed of two elements: fiber reinforcement and SMP matrix consisting of rubber and glass phase, and the volume fraction of each phase will gradually change with the

change of temperature. Ultimately, the constitutive model was tested and verified [9]. Bodaghi et al. studied the thermodynamic behavior of SMP with 4D printing technology and established a constitutive model for verification, and the research results have made outstanding contributions to the study on the mechanical behavior of SMP [10–12]. The thermodynamic constitutive equations on SMP are of great guiding significance for the investigation on the shape memory effect.

Casing of oil and water well is an important part of oilfield production system, and its integrity is an important guarantee for the normal production of oil and water wells. Damaged casings in oil and water wells will result in imperfect injection-production well patterns and destroy injection-production correspondence. However, water flooding loss and recoverable reserves are important factors affecting stable oil production to varying degrees. Casing subsidy technology is one of the effective measures for casing damaged wells. The traditional method is to run the steel casing into the damaged section of the casing downhole, and make the steel casing plastically deformed by hydraulic expansion and cold extrusion to satisfy the required size, thus subsidizing the damage to the inner wall of the casing for restoring the integrity of the casing. The technology has the advantages of high strength

* Corresponding authors.

E-mail addresses: dakun2008@163.com (Z. Ren), sunyl_cq@petrochina.com.cn (Y. Sun), lqw_cq@petrochina.com.cn (Q. Li), yihua_cq@petrochina.com.cn (L. Yang), liuliwu_006@163.com (L. Liu), yj_liu@hit.edu.cn (Y. Liu), lengjs@hit.edu.cn (J. Leng).

<https://doi.org/10.1016/j.compstruct.2021.114331>

Received 17 April 2021; Revised 17 June 2021; Accepted 29 June 2021

Available online 3 July 2021

0263-8223/© 2021 Elsevier Ltd. All rights reserved.

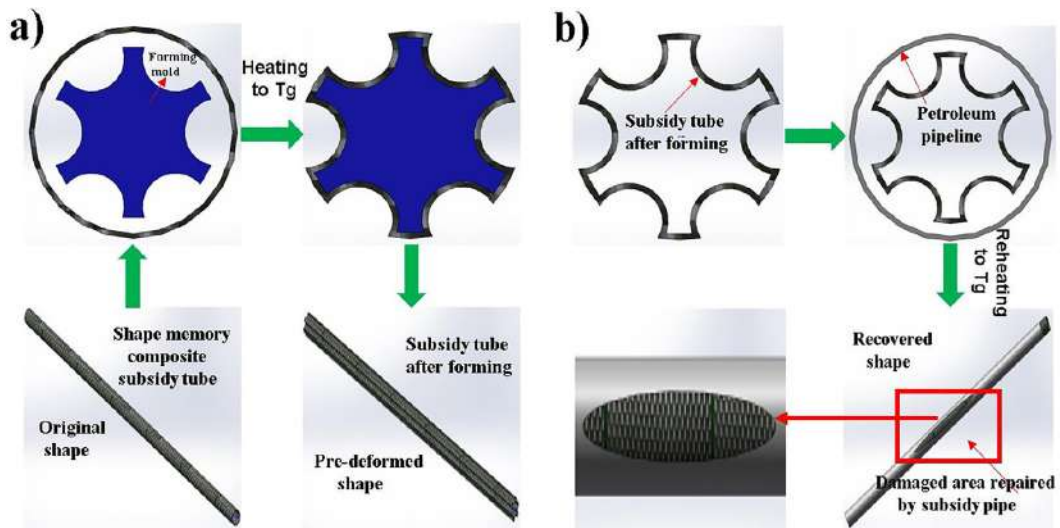


Fig. 1. (a) Schematic diagram of subsidy pipe forming process; (b) Schematic diagram of subsidy pipe plugging damaged pipeline.

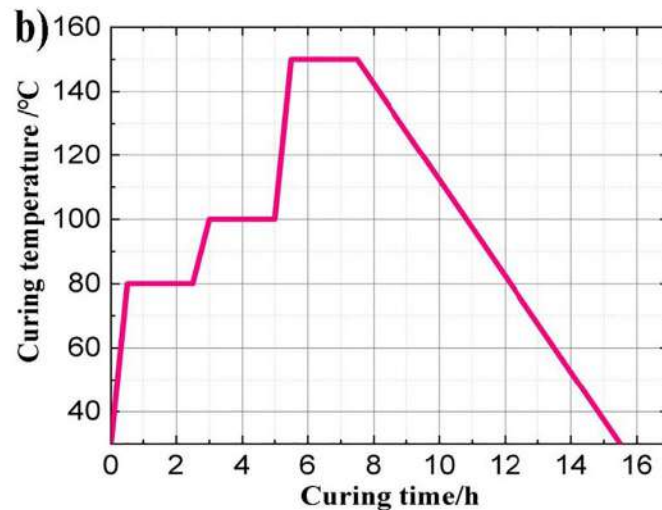
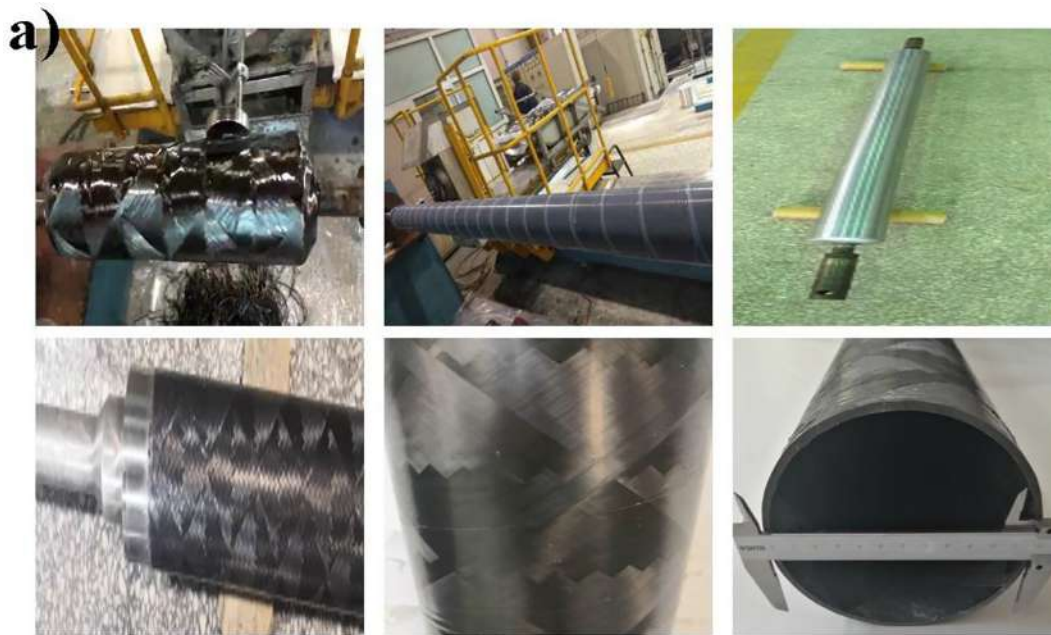


Fig. 2. (a) Manufacturing and processing drawing of subsidy pipe; (b) The curing cycle of SMPC.

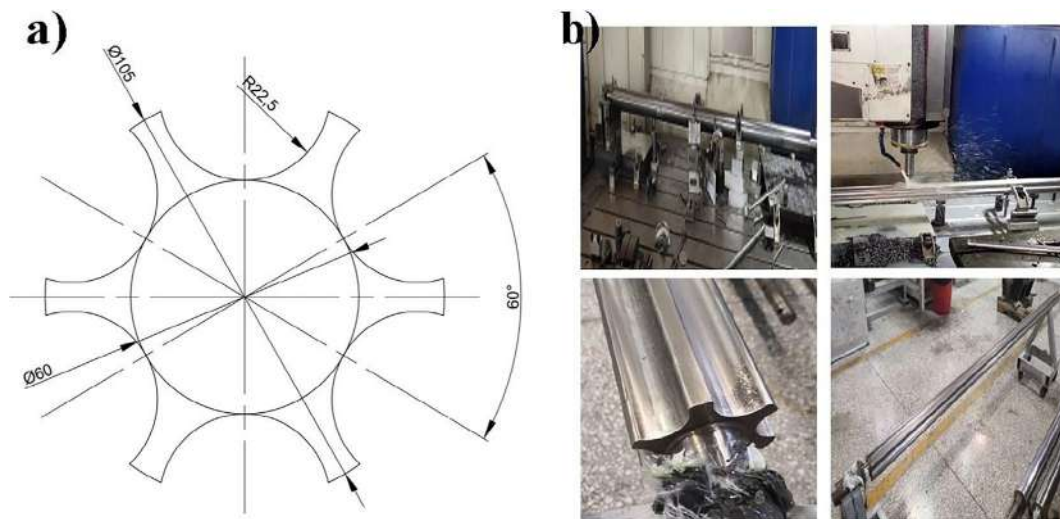


Fig. 3. (a) Sectional dimension drawing of mold; (b) Diagram of forming mold manufacturing.

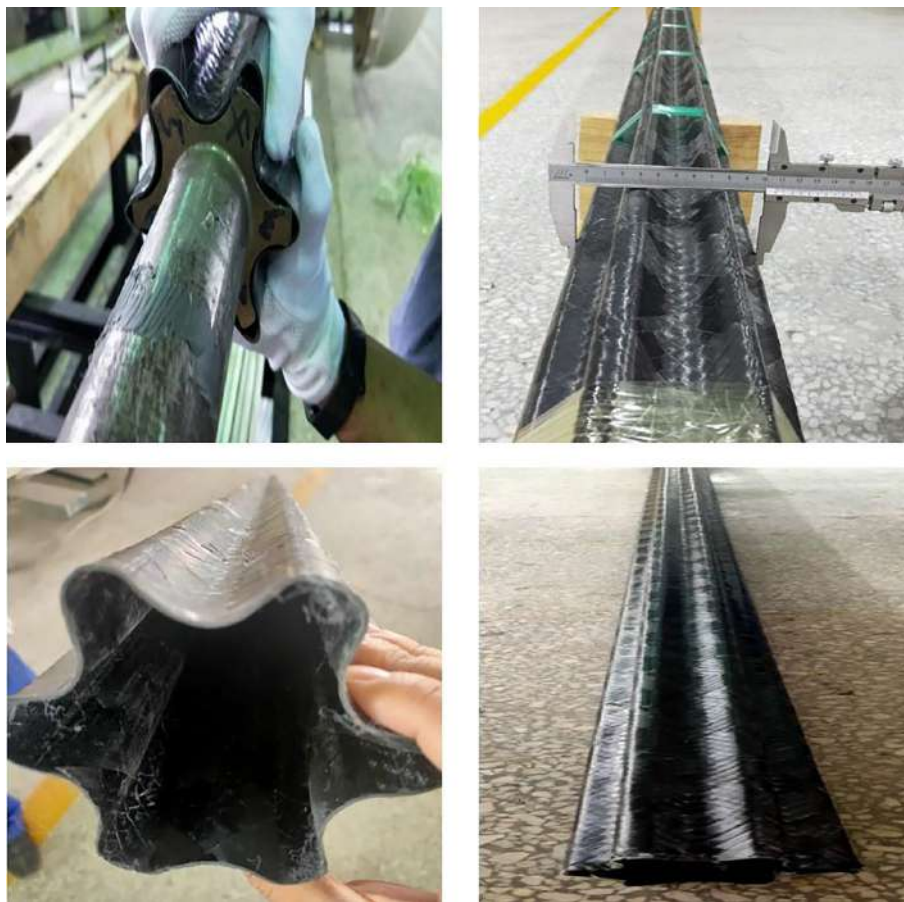


Fig. 4. Subsidy pipe management after forming.

and high temperature resistance but has problems such as low success rate, high cost, and high construction risk.

SMPC are widely used in the field of petroleum engineering. The packer based on SMPC, made by Baker Hughes Corporation, can be used to meet the requirements of the open hole plug in the pipeline, while the polyurethane foam developed below the mine can meet the specific requirements of a variety of environments [13–17]. Hu et al. introduced a kind of thermosetting high-density polyolefin, such

as high-density polyethylene (HDPE), polytetrafluoroethylene (PTFE) as SMP. The composite formed by adding reinforcement phase material into the SMP can be applied to prepare an expandable and deformable packer rubber barrel for plugging damaged pipelines [18,19]. Mansour et al. analyzed the application of SMP in drilling fluid plugging agent, and specifically investigated the performance of intelligent plugging drilling fluid at different temperatures and pressures [20]. Taleghani et al. analyzed the shape memory expandable cement slurry



Fig. 5. Shape recovery diagram of subsidy tube.

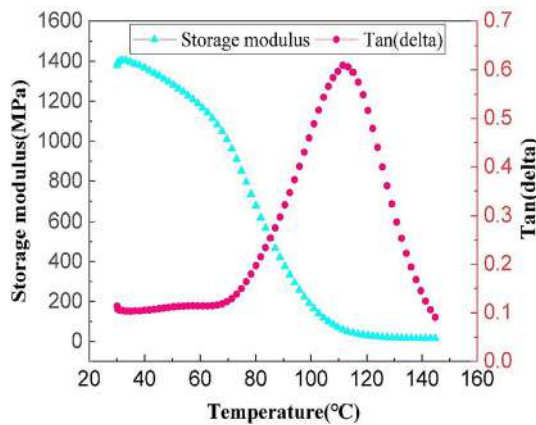


Fig. 6. Storage modulus and tangent delta versus temperature of pure SMP.

aiming at the problem of cement shrinkage and failure in the process of setting in oil and gas wells, and found that SMP could maintain a fixed shape at room temperature and quickly return to the initial shape when the temperature was raised to T_g , thus achieving the purpose of plugging [21]. Santos et al. verified the conductivity characteristics of intelligent expansive proppant, and found that intelligent expansive proppant could maintain or increase fracture width by expandable stress release after external excitation [22]. Osunjaye et al. developed a shape memory sand control screen pipe to replace the traditional open hole gravel packing completion technology, and sand control screen used for heating and compression had an SMP diameter slightly larger and lower than the wellbore diameter. SMP was stimulated by external heating and returned to the original size after it was placed in the specified location, fitting well with the wellbore to block the sand with different particle sizes [23].

The traditional method for repairing pipeline is to coat the damaged part of the pipeline with carbon fiber or glass fiber surface, and determine the number of layers according to the pressure of the damaged part of the pipeline. However, it is difficult to achieve its purpose if the damaged pipeline cannot be artificially wound. In addition, as

the damaged parts of underground pipelines are relatively dispersed, there are lots of damaged holes, so it is necessary to study a process method that can block the damaged holes in a large area.

Compared with the repair methods developed by other researchers, this paper proposes for the first time the use of carbon fiber toughened epoxy resin-based SMPC as the material for repairing downhole casing. The method can overcome the difficulties of underground operation, and solve the problem that the damaged holes are scattered and difficult to plug. Furthermore, the SMPC subsidy tube prepared in this paper has the advantages of large deformation, high specific strength and specific rigidity. The SMPC subsidy pipe (length: 3 m) prepared in this study has a large length dimension, which can plug the oil pipeline in the same length of the damaged area downhole, which has never been attempted by other researchers. It can overcome the difficulty that the underground oil pipeline cannot be repaired after damaged.

2. Design and fabrication of integrative SMPC subsidy pipe

In this paper, according to the specific requirements of the project, the subsidy pipe based on SMPC was designed and manufactured, and the epoxy resin-based material with shape memory effect was provided by Jinsong Leng's group, and the glass transition temperature was ca. 100 °C [24]. Fig. 1 describes the molding process of the subsidy pipe and the principle of plugging the damaged pipeline, namely, the original size of the subsidy pipe has a larger outer diameter, which, however, is reduced after molding. When the shaped pipe is put into the damaged pipeline, the shape of the pipe rebounds after external excitation, forming a close fit with the damaged pipeline to play a role of plugging.

In this study, carbon fiber was directly wound on the mandrel after dipping by wet winding method. The advantages are simpler process, less fiber damage and fewer pore defects. The processing process is shown in Fig. 2(a). The wound subsidy pipe was heated and cured in an oven. The curing temperature and time are shown in Fig. 2(b), namely 80°C/3h, 100°C/3h, and 150°C/5h. After the curing gradient was completed, the sample temperature was gradually reduced to room temperature. The carbon fiber (T700) was wound on the steel ($\pm 45^\circ$ along the axis). The product produced by this process demon-

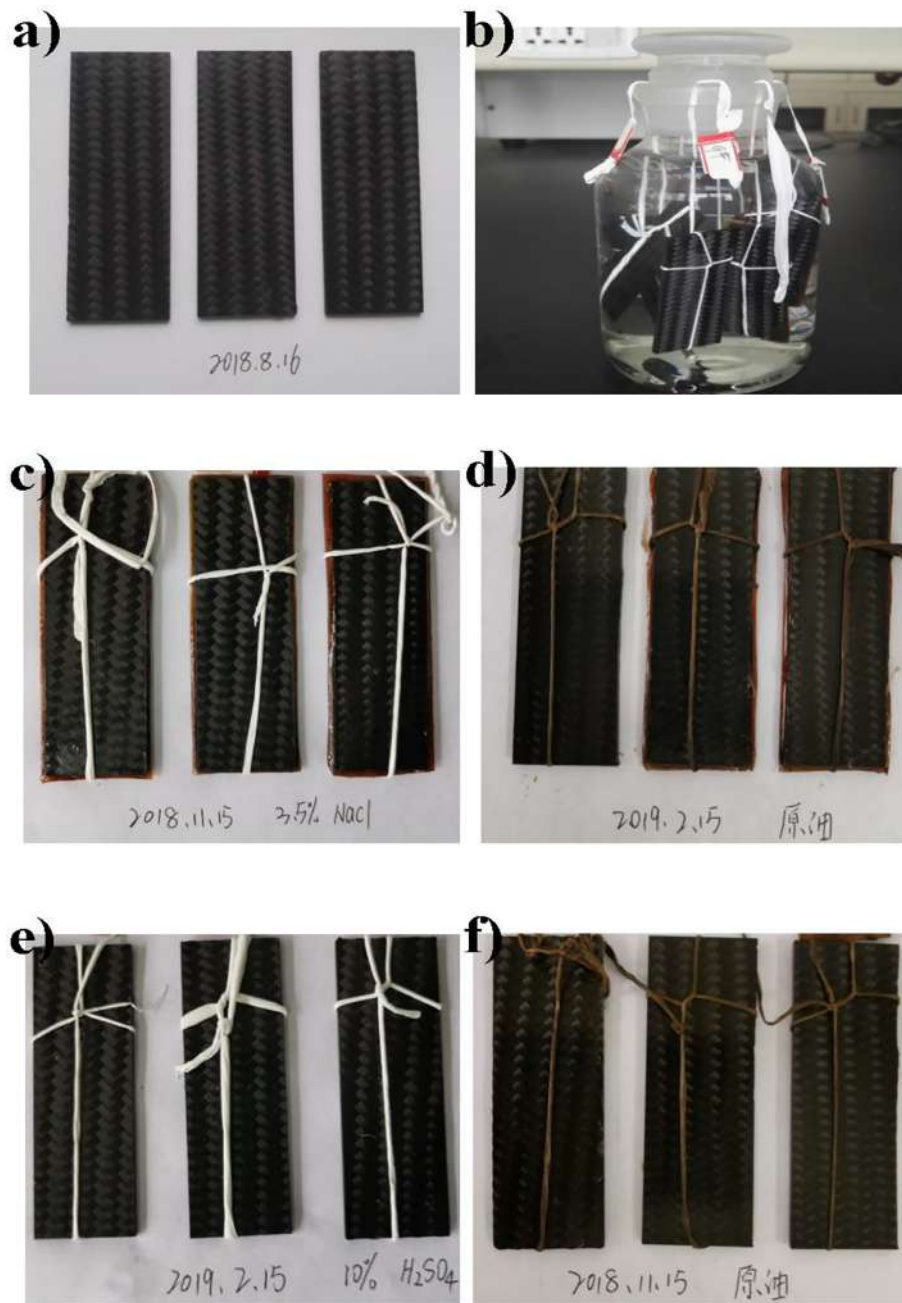


Fig. 7. Morphology of SMP composites after immersion in chemical medium, (a) the original appearance of SMPC; (b) SMPC in corrosive media; (c) placed in 3.5% NaCl solution for 90 days; (d) placed in crude oil for 180 days; (e) placed in 10% H_2SO_4 solution for 180 days; (f) placed in crude oil for 90 days.

strated high rigidity and could fulfill the strength requirements. In this project, the size of the subsidy pipe is given (that is, outer diameter/126 mm, inner diameter/123 mm, and length/3m).

2.1. Forming mold manufacturing

According to engineering requirements, the initial outer diameter of the subsidy pipe was set to be 126 mm so as to withstand a pressure of 10 MPa. Due to the requirements of installation tooling, the outer diameter of the molding subsidy tube cannot exceed 108 mm. In the meantime, the diameter of the central area of the forming subsidy tube should be at least 60 mm to ensure that the installation tool has enough space to work. According to the above requirements, the design and machining process of the tool are introduced in this paper.

Fig. 3(a) is the cross-sectional dimension diagram of the forming mold designed according to the requirements, and the cross-sectional form in **Fig. 3(a)** was designed to meet the corresponding requirements of the project. The field drawing of mold manufacturing is shown in **Fig. 3(b)**. As the mold is long and the cross-sectional area is relatively low, it is easy to vibrate during the processing, which affects the straightness of the specimen. The mold was made of Q345 steel with high strength.

2.2. Shape recovery test of subsidy pipe

The appearance and dimension are shown in **Fig. 4**. The outer diameter of the subsidy pipe after successful molding was 108 mm, which met the engineering requirements. In the downhole, the subsidy

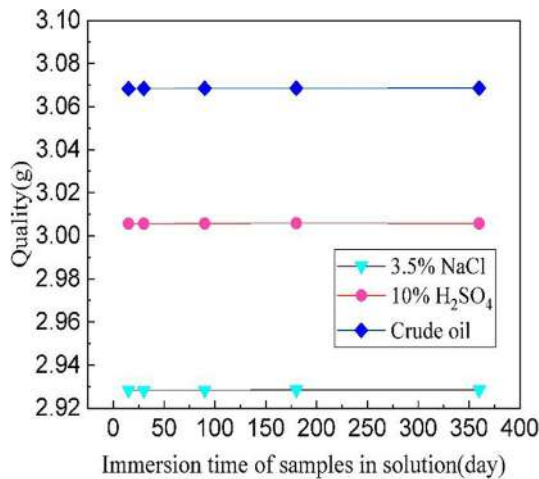


Fig. 8. Quality of samples after immersion in chemical medium.

pipe was placed in the designated position by positioning and installation tools, while the downhole water was heated to the desired temperature with a heating belt to ensure that the shape of the subsidy pipe can rebound.

The resilience test process of the subsidy pipe is shown in Fig. 5. The subsidy pipe with an outer diameter of 126 mm was put into the damaged pipeline with an inner diameter of 124 mm. The subsidy pipe and the damaged pipeline were placed in a water bath with a temperature of 90 °C. The subsidy pipe formed a close fit with the pipeline after it rebounded.

3. Experiments

3.1. Dynamic mechanical analysis

The glass transition temperature of SMP and SMPC was tested using Dynamic Mechanical Analysis (DMA) [25–26]. Due to the shape memory effect of the epoxy resin used in this study, the modulus of SMP changed with the change of temperature, especially in the glass transition temperature region. SMP changed from glassy state to rubbery state. In addition, the polymer gradually changed from high elasticity to viscous fluidity, and the modulus was greatly reduced, especially at the critical point of the glass transition temperature, because the state of the polymer changed to viscous flow state, with the ratio between the loss modulus and the storage modulus (the loss angle) being the highest. In this paper, the dimensions of the sample were 30 mm × 4 mm × 1.95 mm, the test temperature was increased from 25 °C to 200 °C, the heating rate was 3 °C/min, and the loading frequency was 1 Hz.

Table 1

Thickness of samples after immersion in chemical medium.

Sample thickness(mm)					
Immersion time (day)	15d	30d	90d	180d	360d
3.5%NaCl	2.02	2.02	2.02	2.02	2.02
10% H ₂ SO ₄	2.02	2.02	2.02	2.02	2.04
Crude oil	2.02	2.02	2.02	2.02	2.04

Table 2

Temperature and pressure corrosion test medium.

K ⁺ + Na ⁺	Ca ²⁺	Mg ²⁺	CO ₃ ²⁻	HCO ₃ ⁻	SO ₄ ²⁻	Cl ⁻	Salinity	PH	Water type
8400	7800	170	0	70	760	19,800	37,000	6.8	CaCl ₂

3.2. Corrosion resistance and temperature–pressure test

In this study, the subsidy pipe was placed downhole, and the liquid in the wellbore contains many corrosive components that are affected by certain pressure and temperature. Therefore, it is necessary to conduct corrosion resistance and temperature–pressure tests on the SMPC material for evaluating the influence of the above factors on SMPC materials.

The resistance of SMPC to chemical media was evaluated with reference to GB/T 3857 *Test Method for Chemical Resistance of Glass Fiber Reinforced Thermosetting Plastics*. The SMPC test pieces were soaked in 10% HCl solution, 3.5% NaCl solution and crude oil respectively for 90 days. The test pieces must be perpendicular to the horizontal plane and parallel to each other, with a spacing of at least 6.5 mm. The edge of the test piece should be at least 13 mm away from the container or page. Whether the sample discoloration occurred and whether there was any precipitation, cracks, loss of gloss, corrosion, bubbles, softening and other defects on the surface of the samples were observed after the samples were soaked. After the samples were rinsed with running water, the surface moisture was removed with a filter paper, and then stored at room temperature and normal humidity (45%–75% relative humidity) for 30 min. The quality, size (length, width and thickness), bending strength and modulus of the samples were tested.

The 17005D high-temperature autoclave corrosion test system of American Cortest was used to simulate the actual working conditions of the oil field and test the effect of temperature and pressure on the performance of the SMP subsidy pipe.

The temperature and pressure test conditions were: total pressure 6 MPa, temperature 70 °C, and test time 168 h. It was evaluated with reference to GB/T7901 *Metal Material Laboratory Uniform Corrosion Full Immersion Test Method*. The stripe samples with the size of 65 mm × 25 mm × 3 mm was prepared. The samples were placed vertically in the autoclave, and the liquid medium was slowly poured into the autoclave without contact between the samples with the wall of the autoclave. The lid of the autoclave was closed tightly, and temperature was raised after 30 min of nitrogen deoxygenation. The pressure and temperature in the kettle were maintained at the specified values, and the test lasted for 168 h. The autoclave was naturally cooled down, the pressure in the autoclave was reduced to normal pressure within 30 min at a constant speed, and then the samples were taken out. After the test, the appearance and integrity of the samples were observed to see whether there were failure characteristics such as shedding, bubbling, swelling, etc., and compare the test with the untested samples to calculate the swelling rate of the SMPC material.

3.3. Tensile experiments of SMPC

Mechanical experiments were carried out on five kinds of tests, including 3.5% NaCl immersion for 1 year, temperature and pressure



Fig. 9. Morphology of SMPC before and after temperature and pressure test.

Table 3
Corrosion rate and swelling rate of SMPC.

Sample number	Sample quality before test (g)	Sample quality after test (g)	Swelling rate (%)
1	5.8108	5.8174	0.1136
2	4.9082	4.908	-0.0041
3	5.2258	5.2311	0.1014

resistance, crude oil immersion for 1 year, 10% sulfuric acid immersion for 1 year, and unsoaked control samples, to compare the corresponding elastic modulus and tensile strength. Zwick testing machine was used for the test, with ASTM-D3039 as the standard.

3.4. SMPC subsidy pipe withstanding stress test

In order to evaluate the pressure bearing capacity of the SMPC subsidy pipe in the wellbore, a ground simulation evaluation test was carried out, and the internal and external pressure of the SMP composite subsidy pipe was tested by ground high pressure detection equipment. The required tools and equipment are as follows: 5½" casing short joint (1.1 m in length, 4 holes with a diameter of 4 mm, 2 diameter circular holes with diameter of 9 mm), and SMPC subsidy pipe (0.9 m in length). A dead plug was installed on one end (lower end) of the casing sub-subsidized with SMPC subsidy pipe, and a pressure plug on the

other end (upper end). Moreover, liquid (tap water) was pumped from the upper end, according to 2 MPa, 4 MPa, 6 MPa, 8 MPa, suppress 10 MPa step by step, and internal pressure resistance tests were conducted.

The pressure at all levels was stabilized for 5 min, and then was increased by 2 MPa. Then the pressure was released to remove the upper pressure plug. The SMPC subsidy pipe was inspected. In addition, the pressure plug was installed on the upper end of the casing, and the casing nipple was installed into the pressure test tooling. Finally, the external pressure resistance test was carried out step by step according to 1 MPa, 2 MPa, 3MPa, 4 MPa and 5 MPa, that is, each stage was stabilized for 5 min. After the pressure test, the pressure was released to remove the upper and lower dead plug and inspect the SMPC pipe.

3.5. Compression and thermal cycling test of SMPC

The stiffness and elastic modulus of SMPC are affected by carbon fiber content and temperature. In this study, a semi-circular SMPC hinge was prepared. The carbon fiber content of each sample is different, which can be used to refer to the effect of carbon fiber content and experimental temperature on SMPC. The semicircular hinge had an outer diameter of 50 mm and an inner diameter of 30 mm. Carbon fiber fabric was used as the reinforcing phase in SMPC. Each layer of CFRP was 0.25 mm thick, and there were 0 to 10 layers. The effects of different volume contents of CFRP and ambient temperature on the stiffness of SMPC were studied. The SMPC pipe was subjected to axial and radial compression tests at different temperatures. Furthermore, due to the shape memory effect of SMP, a thermal cycle loading test was performed.

4. Result and discussion

4.1. Dynamic mechanical properties of pure SMP

In this paper, the epoxy resin matrix used has the shape memory effect, which arises from the storage modulus and loss factor as a function of the ambient temperature. As shown in Fig. 6, the red curve represents the functional relationship between storage modulus and the temperature, while the blue curve represents that between the ratio of loss modulus to storage modulus (loss factor) and the temperature. The peak of the loss factor is the glass transition temperature (Tg) of the material, hence the Tg of the SMP used in this paper was ca. 110 °C. After the glass transition temperature was reached, the storage

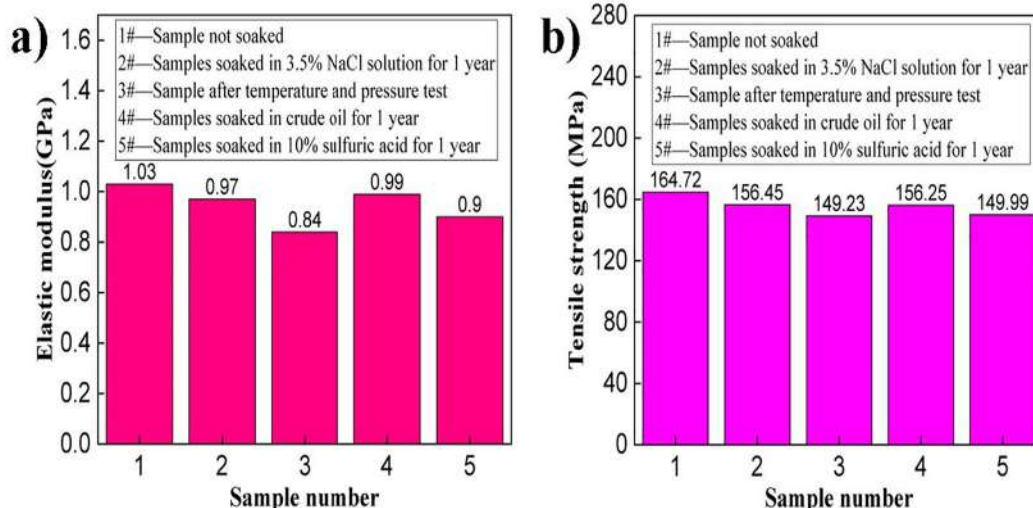


Fig. 10. The elastic modulus (a) and tensile strength (b) of SMPC after immersion in different solutions and temperature and pressure resistance tests.

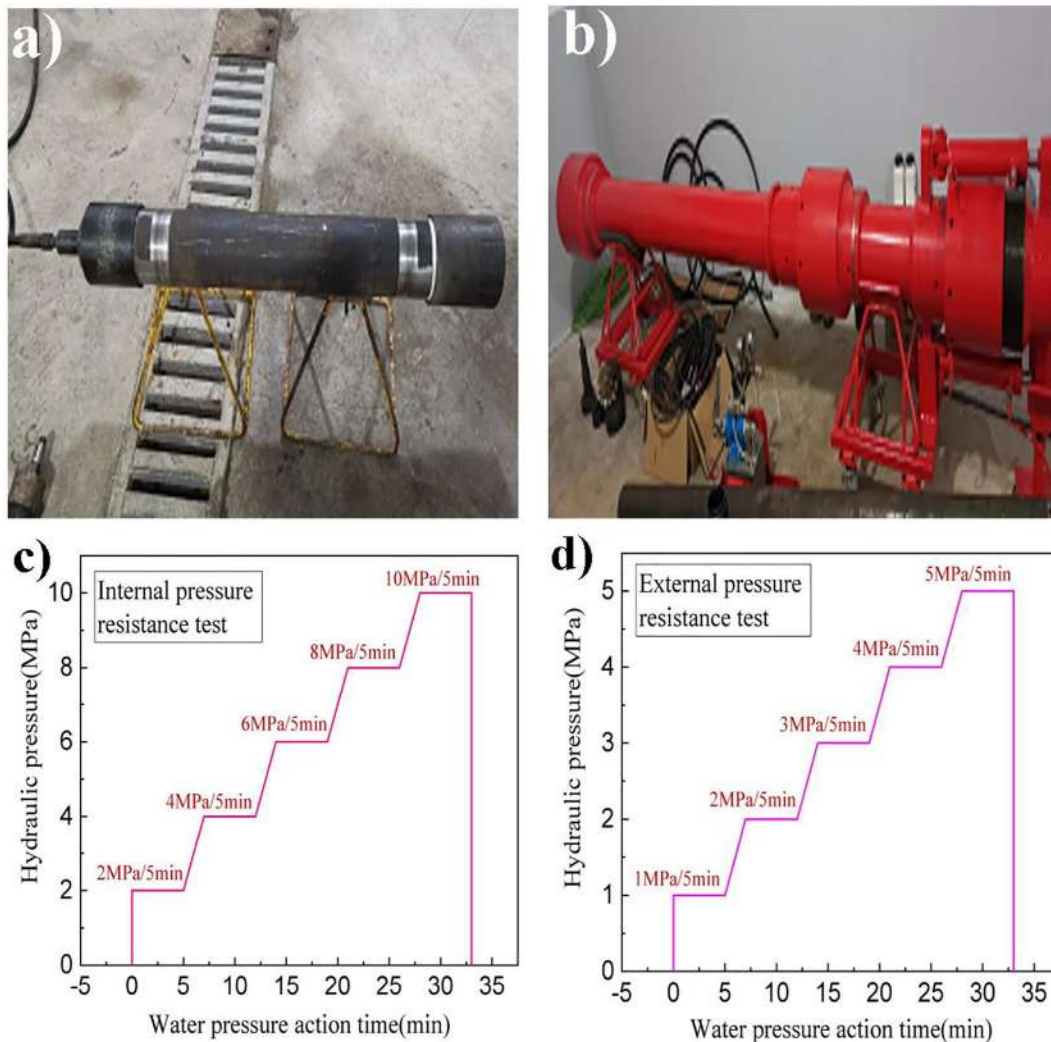


Fig. 11. Pressure test of SMPC subsidy pipe (a) field diagram of internal pressure test; (b) field diagram of external pressure test; (c) pressure gradient curve of internal pressure test; (d) pressure gradient curve of external pressure test.

Table 4
T300/914 Properties of carbon fiber/epoxy [27].

$E_{11}(GPa)$	$E_{22}(GPa)$	$E_{33}(GPa)$	G_{12}	G_{13}	G_{23}	ν_{12}	ν_{13}	ν_{23}
129	9.5	9.8	4.7	4.7	3.2	0.34	0.34	0.52

Table 5
T300/914 Strength parameters of carbon fiber/epoxy [27].

$X_T(MPa)$	$X_C(MPa)$	$Y_T(MPa)$	$Y_C(MPa)$	$S_C(MPa)$
1439	1318	98	215	79

modulus of the material decreased rapidly, suggesting that the material changed from the glassy state with higher modulus to the rubber state, which is an important indicator to measure the shape memory effect.

4.2. Analysis of corrosion resistance and tensile properties of SMPC

As shown in Fig. 7, the appearance of SMPC was observed after 90 days and 180 days in crude oil, 3.5% NaCl solution and 10% H₂SO₄ solution, respectively. There was no obvious change in the appearance of the material.

The effect of soaking days on the quality of SMPC samples in 3.5% NaCl solution, 10% H₂SO₄ solution and crude oil was tested, as shown in Fig. 8. The results showed that the three kinds of solution had no effect on the quality of SMPC. The thickness of the samples was analyzed, as indicated in Table 1. The results are consistent with those in Fig. 8, that is, the thickness of the samples did not change significantly.

Temperature and pressure tests were carried out on the SMPC material, and the components contained in the medium are shown in Table 2. The appearance and morphology of SMPC before and after the test were observed, as displayed in Fig. 9. The samples did not change obviously, without failure characteristics such as foaming, falling off, cracking and swelling. The swelling rate of the samples was tested, as indicated in Table 3. The swelling rate was very small, which was almost negligible, indicating that there was no obvious change in the material. Therefore, SMPC has excellent temperature and pressure resistance.

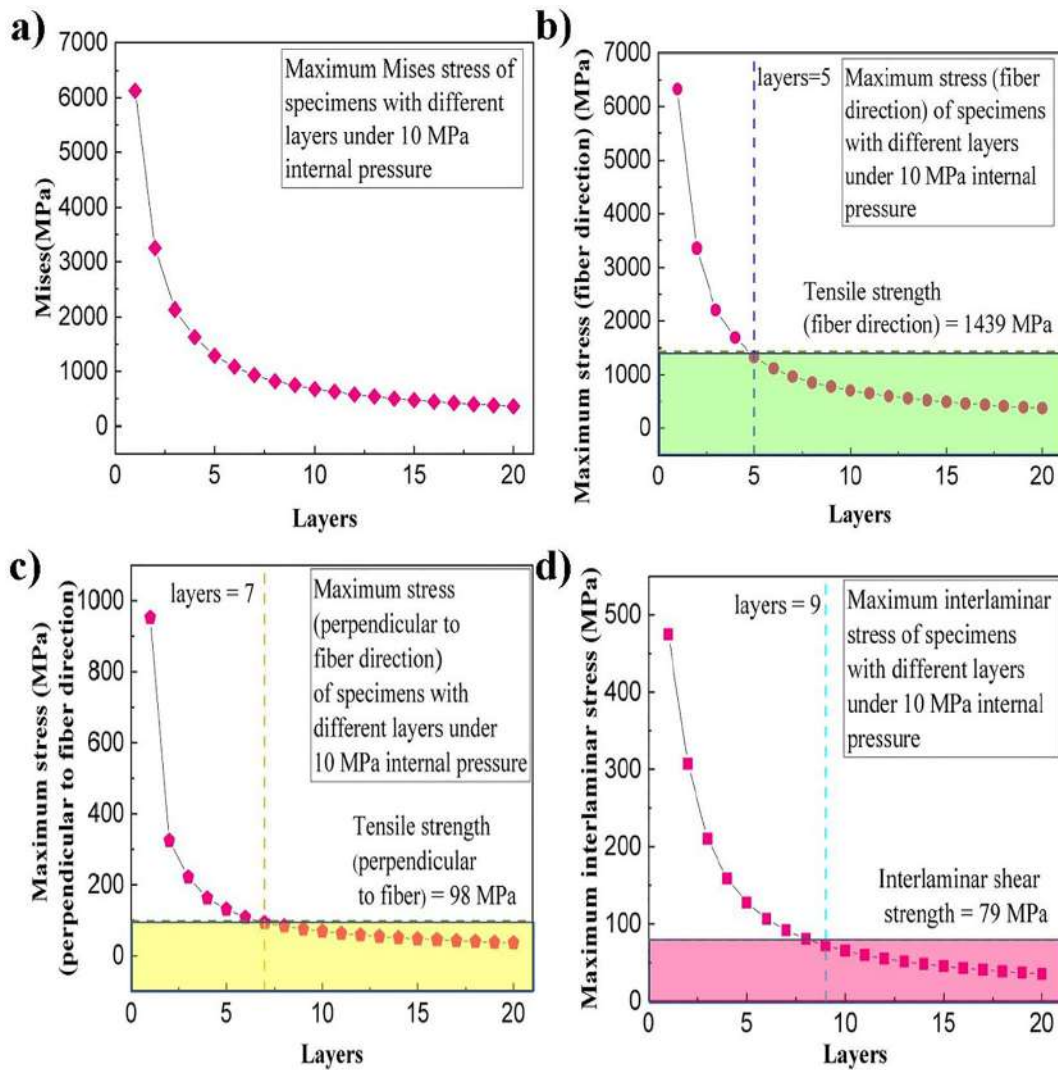


Fig. 12. Maximum stress of samples with different layers under 10 MPa internal pressure: (a) Mises stress; (b) The maximum stress in the fiber direction; (c) Maximum stress perpendicular to the fiber direction; (d) Maximum shear stress.

As shown in Fig. 10, the tensile test was performed on the specimens immersed in 3.5% NaCl solution for 1 year, temperature and pressure resistance, crude oil immersion for 1 year, 10% H₂SO₄ solution for 1 year, and unsoaked specimens. The results indicated that the elastic modulus and strength of SMPC were at a high level after long-term immersion in acid-base, temperature and pressure, and crude oil, indicating excellent stability and environmental resistance.

4.3. Stress test and theoretical analysis of SMPC subsidy pipe

Due to the requirement to plug the damaged holes, the subsidy pipe needs to be able to withstand a certain medium pressure. In this study, the subsidy pipe was tested to withstand internal and external pressure. The test tools for the internal and external pressure of the pipe are shown in Fig. 11(a) and (b), respectively, while the pressure gradient diagrams for the internal and external pressure tests are drawn in Fig. 11(c) and (d), respectively. According to the existing failure theory for simulation analysis, it is necessary to clarify the corresponding material parameters (see Table 4 and Table 5) [27].

The most commonly applied existing failure theories mainly include maximum stress criterion, Tsai-Hill criterion, Tsai-Wu criterion and Hashin criterion [28,29].

1. Maximum stress criterion theory

The stress in the principle direction of the material must be less than the strength in the respective direction, otherwise damage will occur.

The tensile stress can be expressed as:

$$\sigma_1 < X_t, \sigma_2 < Y_t, |\tau_{12}| < S \tag{1a}$$

The compressive stress can be expressed as:

$$\sigma_1 > -X_c, \sigma_2 > -Y_c \tag{1b}$$

where σ_1 — tensile stress in fiber direction; σ_2 — tensile stress transverse to fiber direction; τ_{12} — transverse shear stress; X_t — tensile failure stress in fiber direction; X_c — compressive failure stress in fiber direction; Y_t — tensile failure stress transverse to fiber direction; Y_c — compressive failure stress transverse to fiber direction; S — transverse failure shear.

2. Tsai-Hill criterion theory

Tsai-Hill criterion theory is written as:

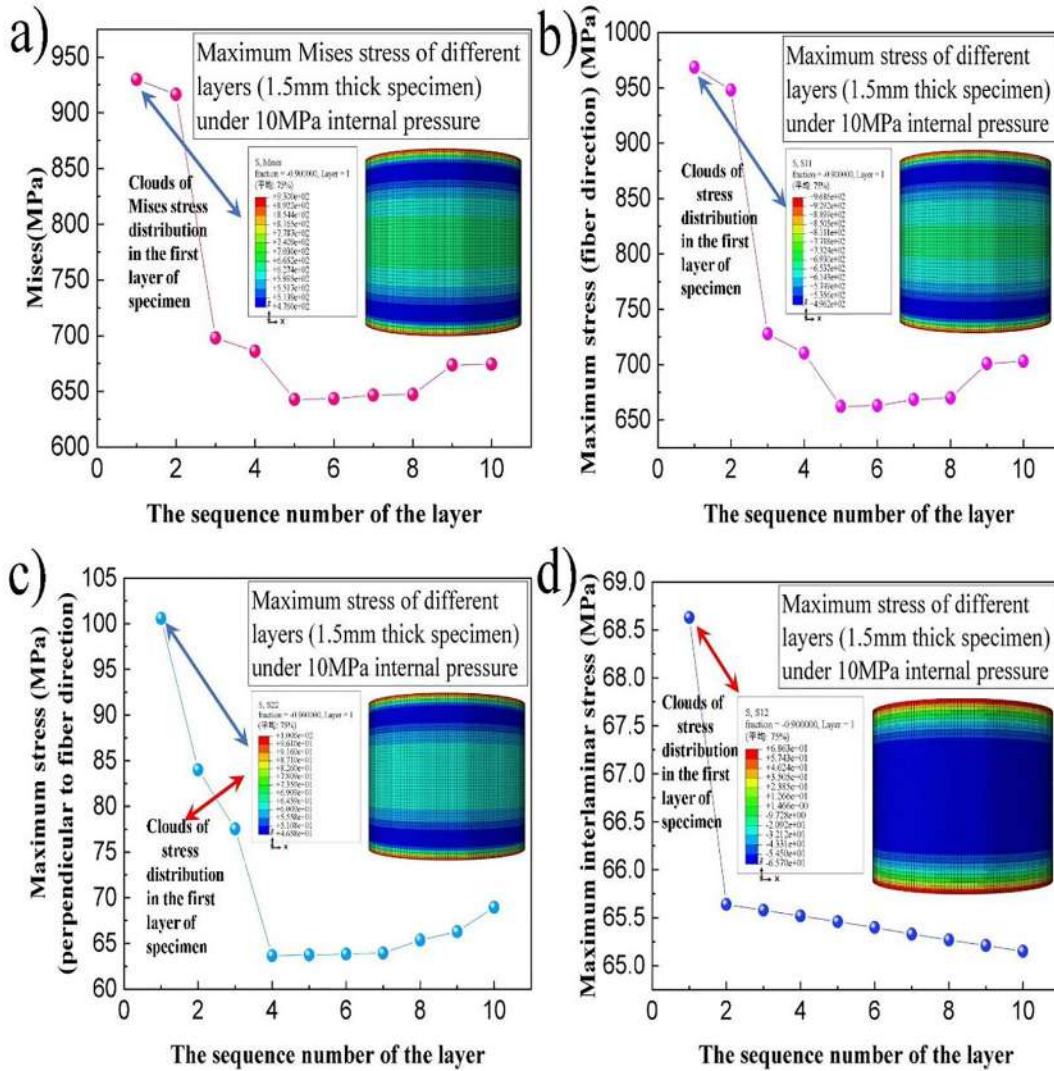


Fig. 13. Maximum stress of each layer of 1.5 mm wall thickness (10 layers) composite pipe under 10 MPa internal pressure, (a) Mises stress; (b) Maximum stress in fiber direction; (c) Maximum stress perpendicular to the fiber direction; (d) Maximum shear stress.

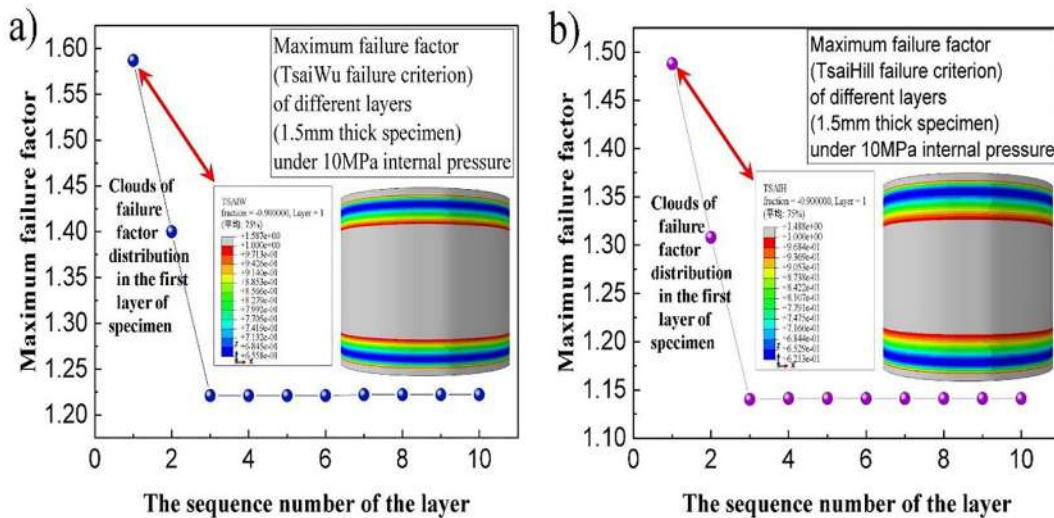


Fig. 14. The maximum failure factor of Tsai-Wu (a) and Tsai-Hill (b) theories for each layer of 1.5 mm wall thickness (10-layer) composite pipe under 10 MPa internal pressure.

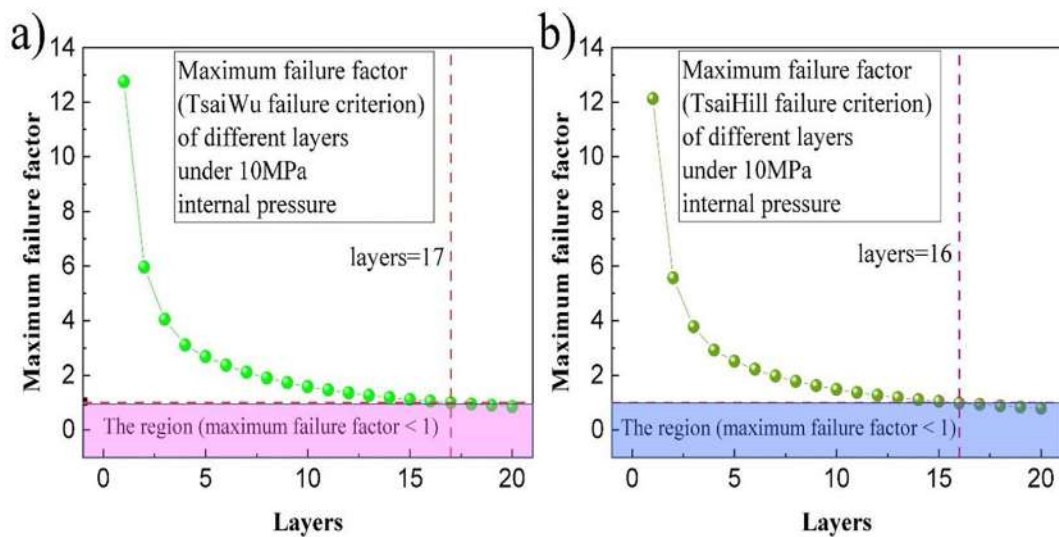


Fig. 15. The maximum Tsai-Wu and Tsai-Hill failure factor of pipes with different layers (thickness) under 10 MPa internal pressure.

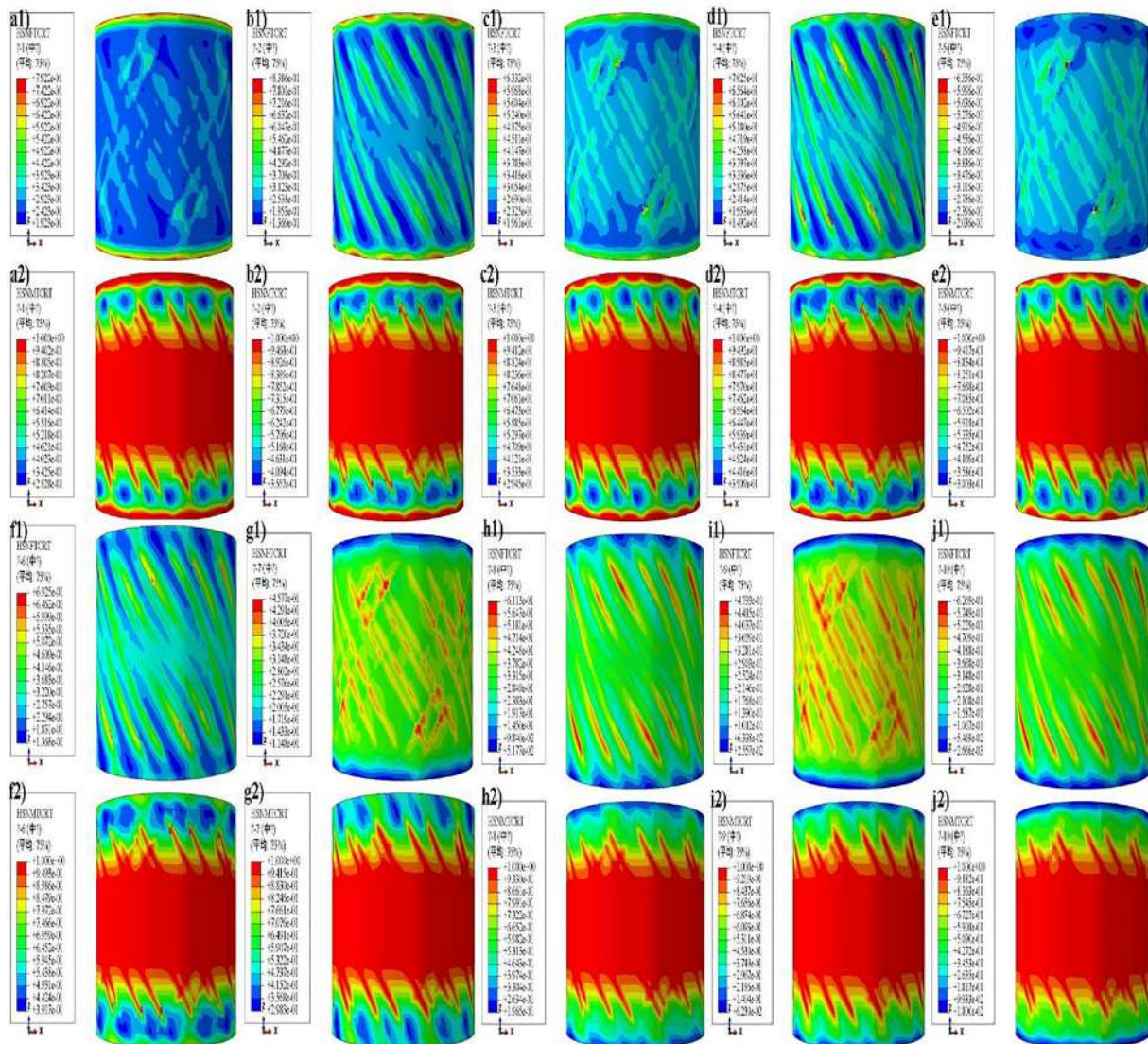


Fig. 16. 1.5 mm wall thickness (10 layers) SMPC pipe under 10 MPa internal pressure: (a1-j1) Hashin failure factor in fiber direction from 1th to 10th layer; (a2-j2) Hashin failure factor in matrix direction from 1th to 10th layer.

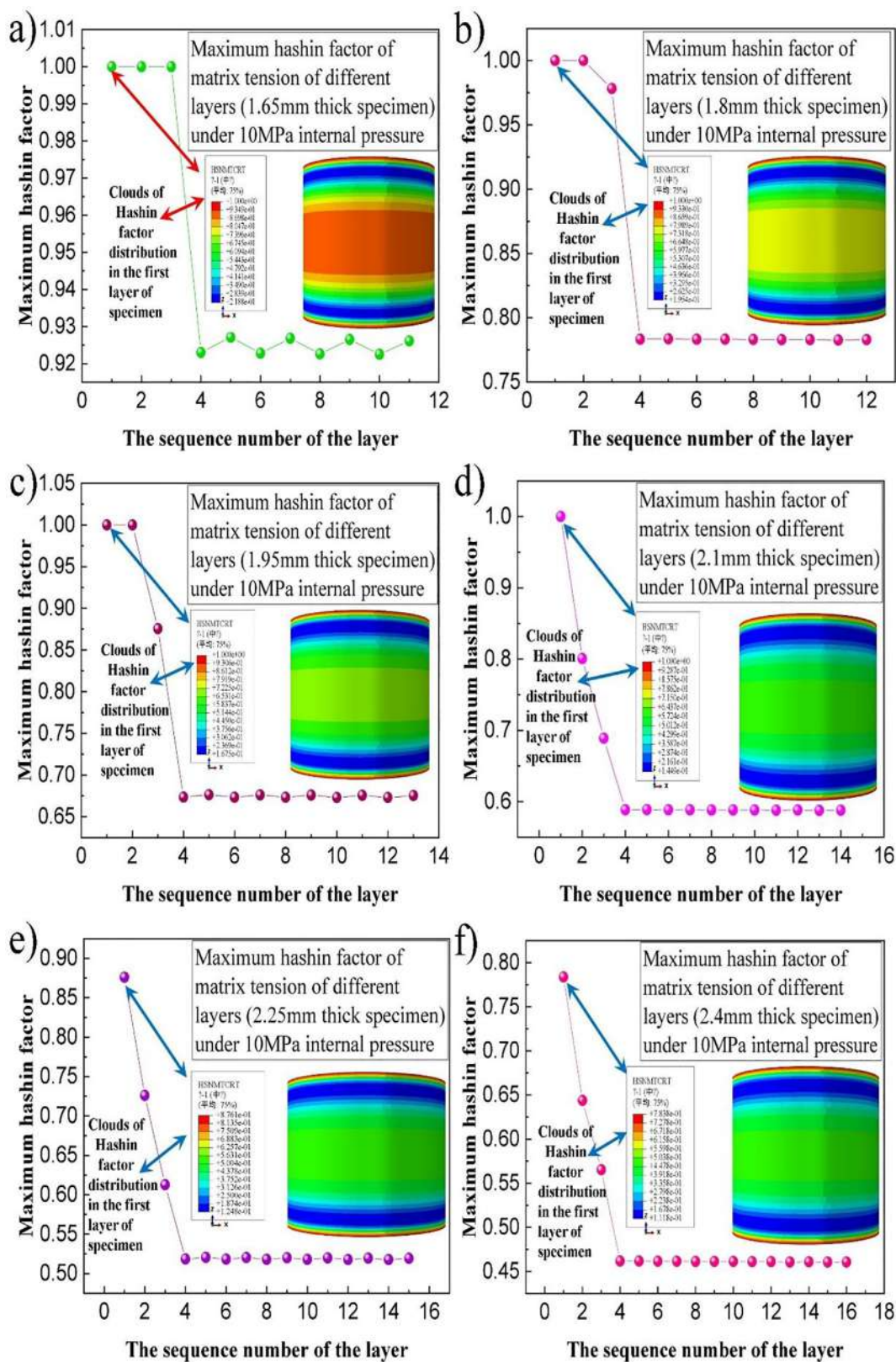


Fig. 17. The maximum Hashin failure factor of each layer with a wall thickness of 11–20 layers under the action of the internal pressure (10 MPa); (a) 11 layers (1.65 mm); (b) 12 layers (1.8 mm); (c) 13 layers (1.95 mm); (d) 14 layers (2.1 mm); (e) 15 layers (2.25 mm); (f) 16 layers (2.4 mm); (g) 17 layers (2.55 mm); (h) 18 layers (2.7 mm); (i) 19 layers (2.85 mm); (j) 20 layers (3 mm).

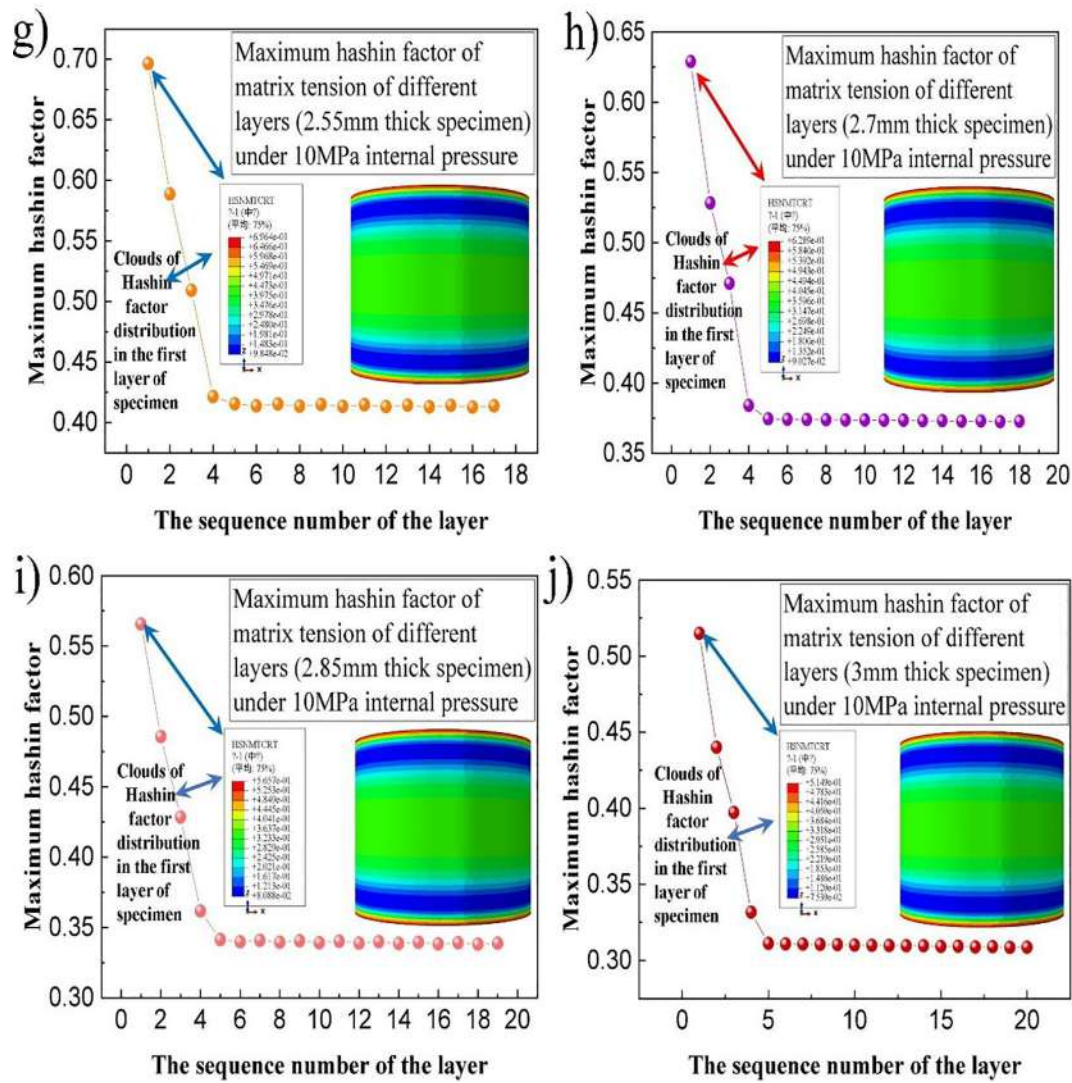


Fig. 17 (continued)

Table 6
Minimum wall thickness to satisfy strength requirements.

	Maximum stress	Tsai-Wu	Tsai-Hill	Hashin
Minimum wall thickness	9 layers (1.35 mm)	17 layers (2.55 mm)	16 layers (2.4 mm)	15 layers (2.25 mm)

$$\frac{\sigma_1^2}{X^2} - \frac{\sigma_1\sigma_2}{X^2} + \frac{\sigma_2^2}{Y^2} + \frac{\tau_{12}^2}{S^2} = 1 \quad (1c)$$

where X —tensile failure stress, Y —compressive failure stress, S —transverse failure shear.

For single-layer composite materials, when Eq (1c) is greater than or equal to 1, the material will be destroyed.

3. Tsai-Wu criterion theory

Tsai-Wu theory is proposed in the form of a tensor, which is expressed as:

$$F_1\sigma_1 + F_2\sigma_2 + F_{11}\sigma_1^2 + F_{22}\sigma_2^2 + F_{66}\sigma_6^2 + 2F_{12}\sigma_1\sigma_2 = 1 \quad (1d)$$

where $F_1 = \frac{1}{X_t} - \frac{1}{X_c}$, $F_{11} = \frac{1}{X_t X_c}$, $F_2 = \frac{1}{Y_t} - \frac{1}{Y_c}$, $F_{22} = \frac{1}{Y_t Y_c}$, $F_{66} = \frac{1}{S^2}$, $F_{12} = \frac{1}{2} \sqrt{F_{11} F_{22}}$.

The strength theory has been extensively applied to engineering. When Eq (1d) is greater than or equal to 1, the material will be destroyed.

4. Hashin criterion theory

The three-dimensional stress failure criterion is expressed as:

Fiber tensile mode ($\sigma_{11} > 0$):

$$\left(\frac{\sigma_{11}}{X_T}\right)^2 + \frac{(\sigma_{12}^2 + \sigma_{13}^2)}{S_{12}^2} = 1 \quad (1e)$$

Fiber compressive mode ($\sigma_{11} < 0$):

$$\left(\frac{\sigma_{11}}{X_C}\right)^2 = 1 \quad (1f)$$

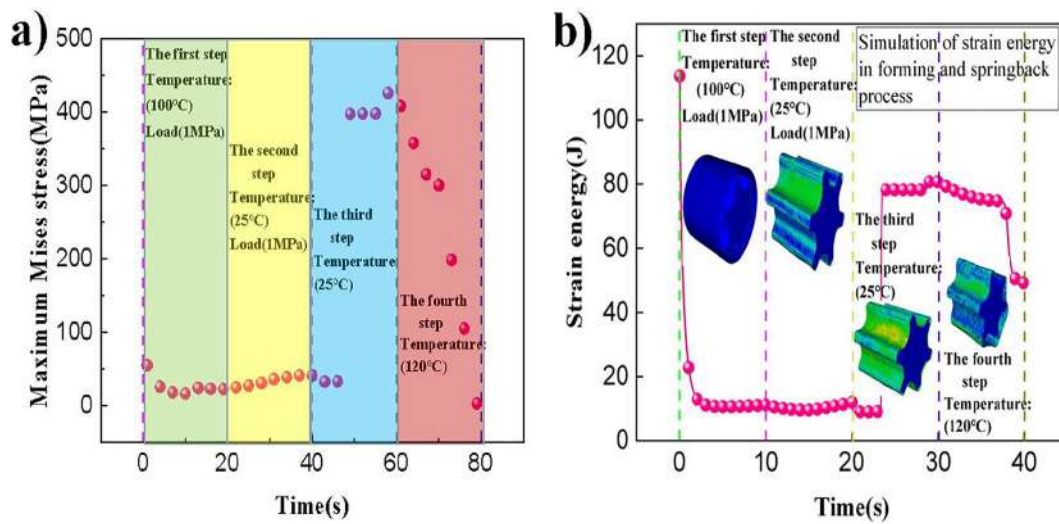


Fig. 18. Simulation of forming and springback process: (a) Maximum Mises stress; (b) Strain energy.

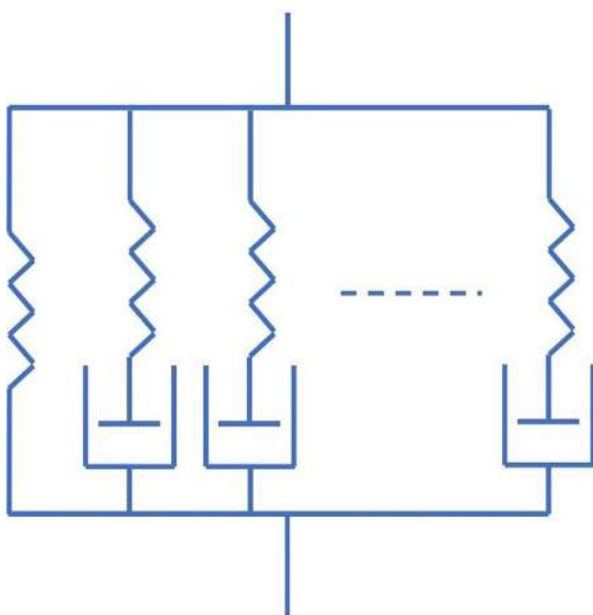


Fig. 19. Thermoviscoelastic constitutive modelling schematic diagram of SMP.

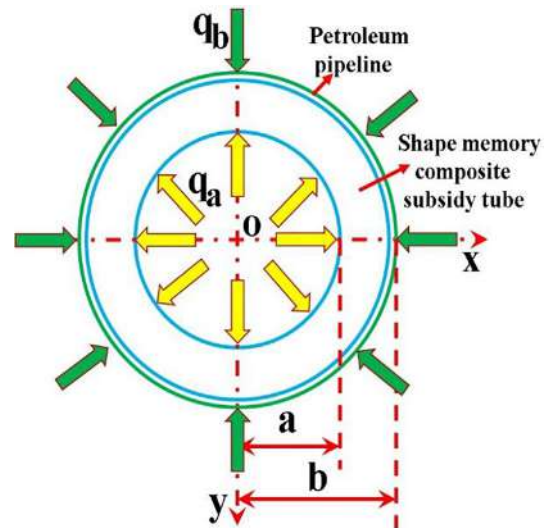


Fig. 20. The pressure state between the subsidy pipe and the damaged pipe.

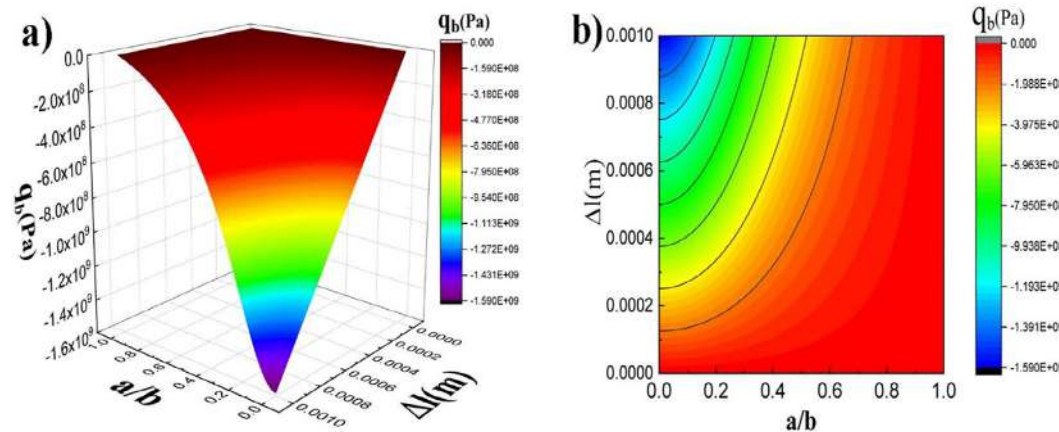


Fig. 21. The external pressure q_b through a/b and ΔL .

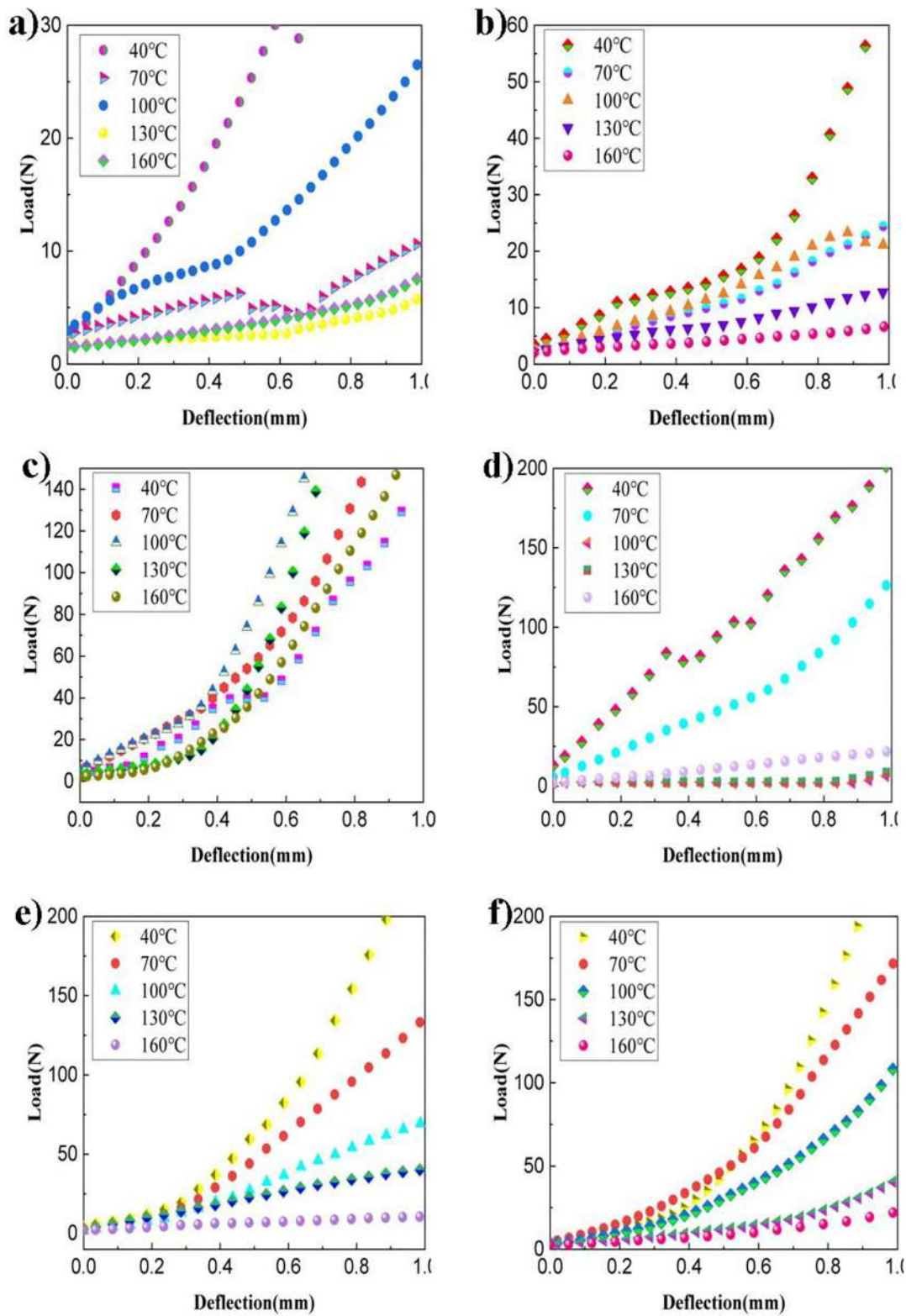


Fig. 22. The functional relationship between deflection and load at different temperatures and carbon fiber content: (a) Pure epoxy resin; (b) one-layer fiber fabric; (c) two-layer fiber fabric; (d) three-layer fiber fabric; (e) four-layer fiber fabric; (f) five-layer fiber fabric; (g) six-layer fiber fabric; (h) seven-layer fiber fabric; (i) eight-layer fiber fabric; (j) nine-layer fiber fabric; (k) ten-layer fiber fabric; (l) the exponential fit function relationship between the number of layers with radial stiffness.

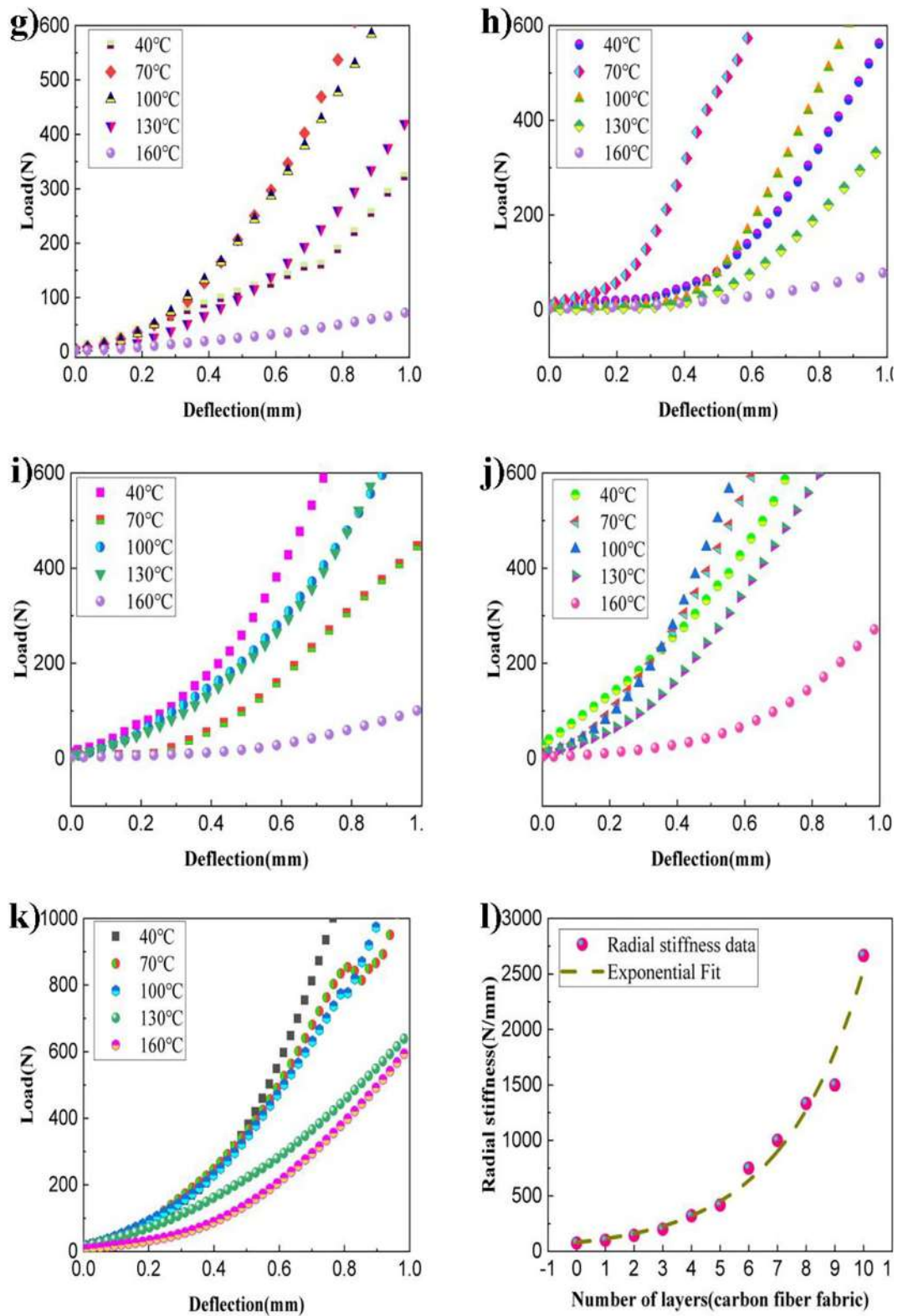


Fig. 22 (continued)

Matrix tensile mode ($\sigma_{22} + \sigma_{33} > 0$):

$$\frac{(\sigma_{22} + \sigma_{33})^2}{Y_T^2} + \frac{(\sigma_{23}^2 - \sigma_{22}\sigma_{33})}{S_{23}^2} + \frac{(\sigma_{12}^2 + \sigma_{13}^2)}{S_{12}^2} = 1 \quad (1g)$$

Matrix compressive mode ($\sigma_{22} + \sigma_{33} < 0$):

$$\begin{aligned} & \frac{\sigma_{22} + \sigma_{33}}{Y_C} \left[\left(\frac{Y_C}{2S_{23}} \right)^2 - 1 \right] + \left(\frac{\sigma_{22} + \sigma_{33}}{2S_{23}} \right)^2 + \frac{(\sigma_{23}^2 - \sigma_{22}\sigma_{33})}{S_{23}^2} \\ & + \frac{\sigma_{12}^2 + \sigma_{13}^2}{S_{12}^2} \\ & = 1 \end{aligned} \quad (1h)$$

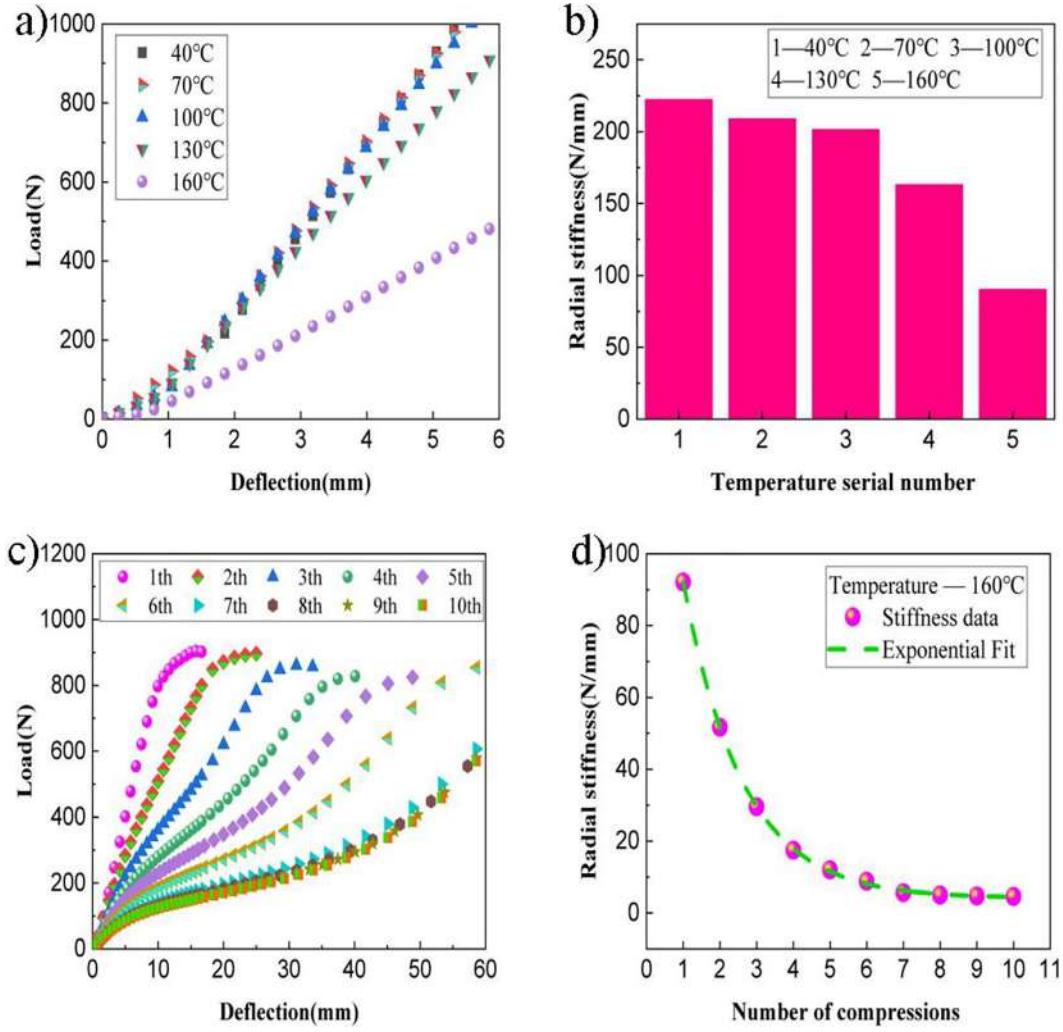


Fig. 23. Radial compression test: (a) Load-Deflection curve at different temperatures; (b) Radial stiffness at different temperatures; (c) Load-Deflection curve at different compression times; (d) Radial stiffness under different compression times.

The plane stress failure criteria is expressed as:

Fiber tensile mode ($\sigma_{11} > 0$):

$$\left(\frac{\sigma_{11}}{X_T}\right)^2 + \left(\frac{\sigma_{12}}{S_{12}}\right)^2 = 1 \quad (1i)$$

Fiber compressive mode ($\sigma_{11} < 0$):

$$\left(\frac{\sigma_{11}}{X_C}\right)^2 = 1 \quad (1j)$$

Matrix tensile mode ($\sigma_{22} > 0$):

$$\left(\frac{\sigma_{22}}{Y_T}\right)^2 + \left(\frac{\sigma_{12}}{S_{12}}\right)^2 = 1 \quad (1k)$$

Matrix compressive mode ($\sigma_{22} < 0$):

$$\frac{\sigma_{22}}{Y_C} \left[\left(\frac{Y_C}{2S_{23}}\right)^2 - 1 \right] + \left(\frac{\sigma_{22}}{2S_{23}}\right)^2 + \frac{\sigma_{12}^2}{S_{12}^2} = 1 \quad (1l)$$

According to the classical laminate theory, the stress analysis of SMPC subsidy pipe under the condition of internal pressure was carried out in this paper, and the corresponding conversion equations are as follows [29]:

$$\begin{bmatrix} \sigma_x \\ \sigma_y \\ \tau_{xy} \end{bmatrix} = T^{-1} \begin{bmatrix} \sigma_1 \\ \sigma_2 \\ \tau_{12} \end{bmatrix} \begin{bmatrix} \sigma_1 \\ \sigma_2 \\ \tau_{12} \end{bmatrix} = T \begin{bmatrix} \sigma_x \\ \sigma_y \\ \tau_{xy} \end{bmatrix} \quad (2a)$$

$$\begin{bmatrix} \varepsilon_1 \\ \varepsilon_2 \\ \gamma_{12} \end{bmatrix} = (T^{-1})^T \begin{bmatrix} \varepsilon_x \\ \varepsilon_y \\ \gamma_{xy} \end{bmatrix} \begin{bmatrix} \varepsilon_x \\ \varepsilon_y \\ \gamma_{xy} \end{bmatrix} = T^T \begin{bmatrix} \varepsilon_1 \\ \varepsilon_2 \\ \gamma_{12} \end{bmatrix} \quad (2b)$$

$$T = \begin{bmatrix} \cos^2\theta & \sin^2\theta & 2\sin\theta\cos\theta \\ \sin^2\theta & \cos^2\theta & -2\sin\theta\cos\theta \\ -\sin\theta\cos\theta & \sin\theta\cos\theta & \cos^2\theta - \sin^2\theta \end{bmatrix} \quad (2c)$$

$$T^{-1} = \begin{bmatrix} \cos^2\theta & \sin^2\theta & -2\sin\theta\cos\theta \\ \sin^2\theta & \cos^2\theta & 2\sin\theta\cos\theta \\ \sin\theta\cos\theta & -\sin\theta\cos\theta & \cos^2\theta - \sin^2\theta \end{bmatrix} \quad (2d)$$

In orthotropic materials, the principal direction of the plane stress state has the following stress-strain relationship:

$$\begin{bmatrix} \sigma_1 \\ \sigma_2 \\ \tau_{12} \end{bmatrix} = \begin{bmatrix} Q_{11} & Q_{12} & 0 \\ Q_{12} & Q_{22} & 0 \\ 0 & 0 & Q_{66} \end{bmatrix} \begin{bmatrix} \varepsilon_1 \\ \varepsilon_2 \\ \gamma_{12} \end{bmatrix} = Q \begin{bmatrix} \varepsilon_1 \\ \varepsilon_2 \\ \gamma_{12} \end{bmatrix} \quad (2e)$$

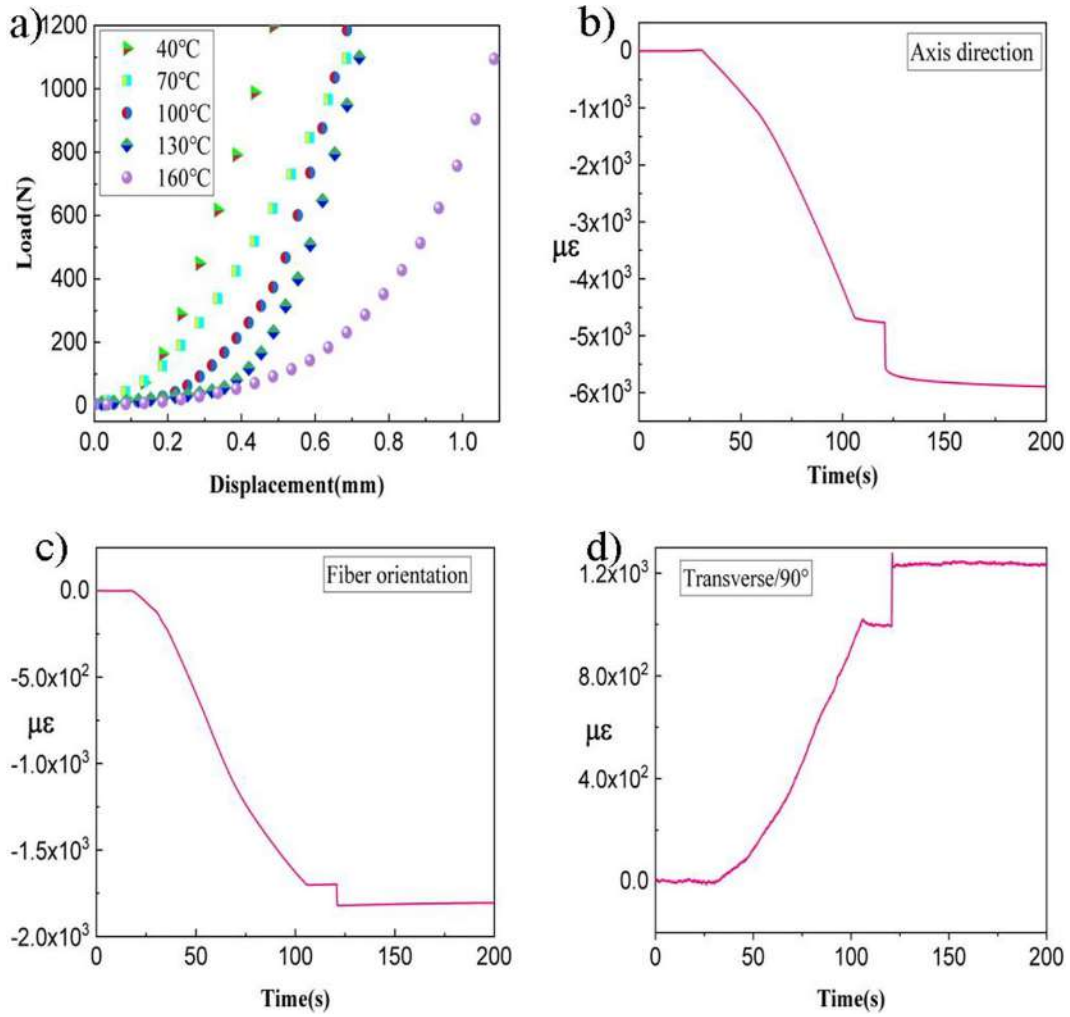


Fig. 24. Axial compression test: (a) Load-Displacement curve at different temperatures; (b) Axial strain–time curve; (c) Fiber direction strain–time curve; (d) Transverse strain–time curve.

After the above equations are derived, the off-axial stress–strain relationship can be obtained:

$$\begin{bmatrix} \sigma_x \\ \sigma_y \\ \tau_{xy} \end{bmatrix} = T^{-1} \begin{bmatrix} \sigma_1 \\ \sigma_2 \\ \tau_{12} \end{bmatrix} = T^{-1} Q \begin{bmatrix} \varepsilon_1 \\ \varepsilon_2 \\ \gamma_{12} \end{bmatrix} = T^{-1} Q (T^{-1})^T \begin{bmatrix} \varepsilon_x \\ \varepsilon_y \\ \gamma_{xy} \end{bmatrix} \quad (2f)$$

The stress–strain relationship in the x-y coordinate can be expressed as:

$$\begin{bmatrix} \sigma_x \\ \sigma_y \\ \tau_{xy} \end{bmatrix} = \bar{Q} \begin{bmatrix} \varepsilon_x \\ \varepsilon_y \\ \gamma_{xy} \end{bmatrix} = \begin{bmatrix} \bar{Q}_{11} & \bar{Q}_{12} & \bar{Q}_{16} \\ \bar{Q}_{12} & \bar{Q}_{22} & \bar{Q}_{26} \\ \bar{Q}_{16} & \bar{Q}_{26} & \bar{Q}_{66} \end{bmatrix} \begin{bmatrix} \varepsilon_x \\ \varepsilon_y \\ \gamma_{xy} \end{bmatrix} \quad (2g)$$

where $\bar{Q} = T^{-1} Q (T^{-1})^T$,

$$\begin{aligned} \bar{Q}_{11} &= Q_{11} \cos^4 \theta + 2(Q_{12} + 2Q_{66}) \sin^2 \theta \cos^2 \theta + Q_{22} \sin^4 \theta, \\ \bar{Q}_{12} &= (Q_{11} + Q_{22} - 4Q_{66}) \sin^2 \theta \cos^2 \theta + Q_{12} (\sin^4 \theta + \cos^4 \theta), \\ \bar{Q}_{22} &= Q_{11} \sin^4 \theta + 2(Q_{12} + 2Q_{66}) \sin^2 \theta \cos^2 \theta + Q_{22} \cos^4 \theta, \\ \bar{Q}_{16} &= (Q_{11} - Q_{12} - 2Q_{66}) \sin \theta \cos^3 \theta + (Q_{12} - Q_{22} + 2Q_{66}) \sin^3 \theta \cos \theta, \\ \bar{Q}_{26} &= (Q_{11} - Q_{12} - 2Q_{66}) \sin^3 \theta \cos \theta + (Q_{12} - Q_{22} + 2Q_{66}) \sin \theta \cos^3 \theta, \\ \bar{Q}_{66} &= (Q_{11} + Q_{22} - 2Q_{12} - 2Q_{66}) \sin^2 \theta \cos^2 \theta + Q_{66} (\sin^4 \theta + \cos^4 \theta), \end{aligned}$$

$$Q_{11} = \frac{E_1}{1 - \nu_{12}\nu_{21}}, \quad Q_{22} = \frac{E_2}{1 - \nu_{12}\nu_{21}}, \quad Q_{12} = \frac{\nu_{21}E_2}{1 - \nu_{12}\nu_{21}} = \frac{\nu_{12}E_1}{1 - \nu_{12}\nu_{21}}, \quad Q_{66} = G_{12},$$

$\frac{\nu_{12}}{E_2} = \frac{\nu_{21}}{E_1}$, θ — off-axis angle, in this study, $\theta = 45^\circ$.

In this study, the tubular structure is subjected to internal pressure, so it is necessary to convert the stress expression in the x-y plane into the stress expression in the cylindrical coordinate system. The stress boundary condition was that the internal pressure was set to be 10 MPa and the external pressure was set to be 0 MPa, and the coordinated continuous displacements of each layer were assumed to be the displacement boundary condition. In addition, the corresponding conversion equations can be referred to the corresponding references [30–33].

The outer diameter of the composite pipe was 126 mm. As the internal pressure was 10 MPa, the wall thickness of the composite pipe needs to be determined according to the material parameters and strength. Therefore, the maximum stress criterion and the finite element software were used for simulation, and the number and thickness of the samples were determined under the condition that the material strength was satisfied. The upper and lower boundary of the subsidiary pipe was set as fixed support, and the six degrees of freedom were set as 0. The simulation results are shown in Fig. 12. Since the thickness of the single-layer carbon fiber composite material was ca. 0.15 mm, the maximum stress distribution of the composite pipe with different layers was summarized, as shown in Fig. 12.

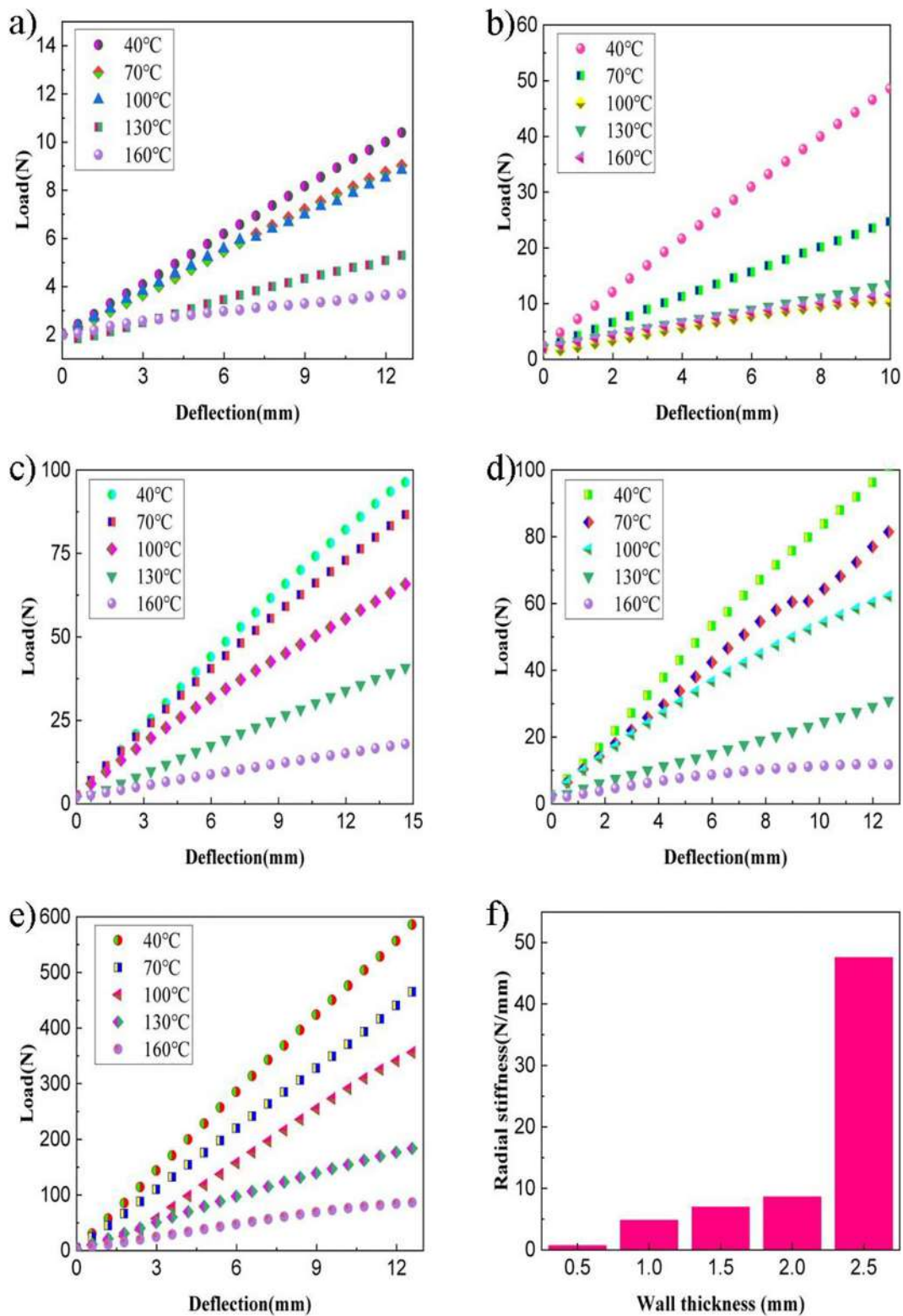


Fig. 25. Load-Deflection curve of radial compression test on the pipes with different wall thickness (outer diameter:126 mm, height: 100 mm): (a) Wall thickness/0.5 mm; (b) Wall thickness/1mm; (c) Wall thickness/1.5 mm; (d) Wall thickness/2mm; (e) Wall thickness/2.5 mm; (f) Radial stiffness.

As the number of layers increased, the maximum stress decreased exponentially. According to the maximum stress criterion, it can be found from Fig. 12(b) that the samples with five layers could satisfy the strength requirement of fiber direction stress, from Fig. 12(c) that

the strength perpendicular to fiber direction could satisfy the strength requirement when there were seven layers, and from Fig. 12(d) that the interlaminar shear strength requirement could be satisfied when there were nine layers. In summary, according to the maximum stress

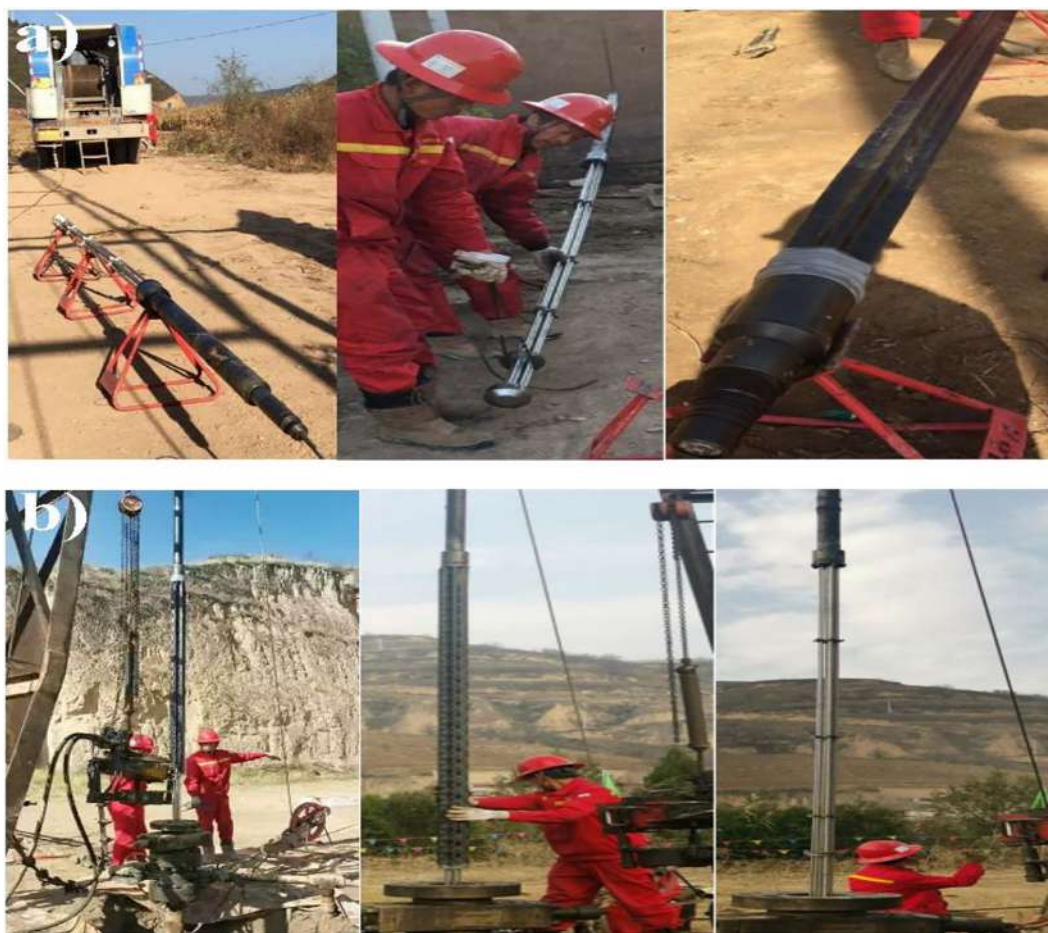


Fig. 26. Subsidy pipe installation: (a) Subsidy pipe surface assembly; (b) Subsidy pipe underground installation.

criterion, there should be at least nine layers, that is, the strength requirement is satisfied when the wall thickness is 1.35 mm, and the wall thickness of the pipe prepared in this paper was 1.5 mm.

After the wall thickness of the pipe (1.5 mm) was determined, the stress distribution of each layer was simulated and analyzed, and the results are shown in Fig. 13. As shown in Fig. 13, the maximum stress of the first layer was the largest. With the increase of the number of layers, the maximum stress of the outer layer continuously decreased. The stress distribution cloud of the first layer is shown in the figure, and the maximum stress basically did not change starting from the fourth layer.

Tsai-Wu and Tsai-Hill criterion are the important basis for identifying material failure. According to the composite pipe with a wall thickness of 1.5 mm determined in this paper, the judgment criteria were used for simulation analysis, as shown in Figs. 14 and 15. Fig. 14 indicates the maximum failure factor of each layer with a wall thickness of 1.5 mm or 10 layers under an internal pressure of 10 MPa. The gray area in the cloud image is the zone where the failure factor is greater than 1 and the material fails. As shown in Fig. 14, the failure area was in the boundary at both ends and the middle area, and the failure factor of the innermost layer was the highest. As the number of layers increased, the maximum failure factor continued to decrease, but basically remained unchanged starting from the third layer.

Fig. 15 shows the trend of the maximum failure factor with different wall thicknesses (number of layers) under an internal pressure of 10 MPa. Tsai-Wu and Tsai-Hill failure criteria were analyzed. According to Tsai-Wu failure theory, when there are 17 layers, the maximum failure factor can be reduced to be less than 1. According to the Tsai-Hill failure theory, when there are 16 layers, the maximum failure fac-

tor can be reduced to be less than 1. Therefore, the judgment results obtained by using these two failure criteria are basically the same, and the wall thickness is higher than the result obtained by the maximum stress criterion.

The Hashin failure criterion was used to simulate and analyze the failure of SMPC pipe with a wall thickness of 1.5 mm under an internal pressure of 10 MPa. The analysis result is shown in Fig. 16, which was mainly caused by the tensile failure in the direction of the matrix. The Hashin failure factor in the middle region of the pipe was generally above 1. However, the fiber direction can withstand the internal pressure owing to the fact that the failure factor is less than 1.

The Hashin failure criterion was used to analyze SMPC pipes with thicknesses of 11–20 layers, as shown in Fig. 17. Under the internal pressure of 10 MPa, when the wall thickness of the pipe was more than 15 layers (2.25 mm), the Hashin failure factor was less than 1, indicating that the strength requirements were satisfied. Compared with the results obtained by Tsai-Wu and Tsai-Hill criteria, the number of layers (wall thickness) obtained is less than that obtained by the above two criteria, but significantly more than that obtained by the maximum stress criterion. As shown in the Hashin failure factor cloud, the largest failure factor was mainly at the fixed-support boundary. And between the first layer and the third layer of SMPC pipes with different wall thicknesses, the maximum Hashin failure factor demonstrated a rapid decline but basically remained unchanged starting from the fourth layer.

Comparing the above failure criteria, different results were obtained. The results of the minimum layer thickness that can satisfy the strength requirements under the internal pressure of 10 MPa are shown in Table 6.

As shown in Table 6, under the internal pressure of 10 MPa, the results about the minimum number of layers (wall thickness) that can satisfy the strength requirements are different among the four criteria.

According to the maximum stress criterion, nine layers are sufficient, but 17 layers is required due to Tsai-Wu criterion, and the number of layers required by Tsai-Hill and Hashin criterion is slightly less than that required by Tsai-Wu criterion. In this paper, the subsidy pipe with a wall thickness of 1.5 mm satisfied the requirements, owing to the strength of the SMPC material in this project being higher than the quoted parameters.

4.4. Simulation analysis and constitutive equation model on SMPC

In this paper, the materials used had a shape memory effect, so the additional incentives rebounded after the subsidy pipe was formed. The formation and rebound process of the subsidy pipe were simulated with reference to the study of Chen Jianguo et al. [34,35]. The maximum Mises stress and strain energy during the forming and rebound of the subsidy pipe were simulated, as shown in Fig. 18. The simulation process mainly includes four steps, each of step was set to 20 s. In the first step, the SMPC subsidy pipe was heated to the glass transition temperature under 1 MPa. The second step was to lower the temperature to 25°C while continuing to apply the load to from the subsidy pipe. The third step was to remove the load while keeping the temperature constant, since the ambient temperature was far below the glass transition temperature, the SMPC was in a glass state and the shape was fixed. In the fourth step, the temperature was increased to the glass transition temperature, and the shape of the subsidy pipe rebounded.

Based on the nonlinear viscoelastic model constitutive theory of SMP, the incompressible Mooney-Rivlin hyperelastic model was used to describe the hyperelastic state of SMP during the glass transition. In the paper, the simulation parameters and constitutive model provided by Chen Jianguo was quoted, and the corresponding schematic diagram of the viscoelastic thermodynamic model is shown in Fig. 19 [35].

The viscoelastic behavior of the SMP in this study is mainly determined by strain-dependent stress and time-dependent relaxation. The corresponding equation is expressed as:

$$\sigma(\varepsilon, t) = \sigma_0(\varepsilon) \cdot g(t) \quad (3a)$$

where the strain response is mainly determined by $\sigma_0(\varepsilon)$, and the relaxation time is primarily represented by the Prony series, which is derived by

$$g(t) = g_\infty + \sum_{i=1}^N g_i \exp\left(-\frac{t}{\tau_i}\right) \quad (3b)$$

where g_∞ and g_i are constants with no dimensions. $g_\infty + \sum_{i=1}^N g_i = 1$. $\sigma_0(\varepsilon)$ symbolizes the relationship between the stress and strain with respect to the material in the first instance. Owing to $g(0) = 1$, the corresponding equation can be deduced and demonstrated, which is $\sigma(\varepsilon, 0) = \sigma_0(\varepsilon)$. Similarly, $\sigma(\varepsilon, \infty) = g_\infty \sigma_0(\varepsilon)$ is inferred by $g(\infty) = g_\infty$. Therefore, $g_\infty \sigma_0(\varepsilon)$ can signify the stress-strain relationship while the relation reaches equilibrium. The movement factor function—WLF (William-Landell-Ferry) equation was quoted in this paper, which is expressed as:

$$-\lg a_T = \frac{C_1(T - T_g)}{C_2 + T - T_g} \quad (3c)$$

The temperature-dependend viscoelastic constitutive equation quoted in this paper is expressed as:

$$\sigma_{ij} = \int_0^t 2G(a_{T,T_r}(t - \xi), T_r)[\dot{\varepsilon}_{ij}(\xi) - \dot{\varepsilon}_{kk}(\xi)\delta_{ij}]d\xi + K\varepsilon_{kk}\delta_{ij} \quad (3d)$$

where T_r —reference temperature; K —Bulk modulus; G —Shear modulus, and the derivative of the strain tensor component signifies the derivative of time ξ . In the paper, $C_1 = 17.44$ and $C_2 = 51.6$.

4.5. Theoretical analysis on the plugging pressure of subsidy pipe

In the paper, the initial outer diameter of the subsidy pipe was 126 mm, and the inner diameter of the damaged pipe was 124 mm. Therefore, when the subsidy pipe was heated and rebounded, a close contact with the damaged pipe was formed, thus generating corresponding pressure. In Fig. 20, the inner radius of the subsidy pipe is a , the outer radius is b , the internal pressure is q_a , and the external pressure is q_b .

According to the related formula of elastic mechanics, the bonding pressure formed between the damaged pipeline and the subsidy pipe was analyzed and calculated, and the related formula is as follows [36].

In polar coordinates, assume that the stress function Φ is only the function of the radial coordinate ρ , i.e. $\Phi = \Phi(\rho)$, and the stress equations are given by

$$\sigma_\rho = \frac{1}{\rho} \frac{d\Phi}{d\rho}, \quad \sigma_\varphi = \frac{d^2\Phi}{d\rho^2}, \quad \tau_{\rho\varphi} = \tau_{\varphi\rho} = 0 \quad (4a)$$

The compatibility equation is $\left(\frac{d^2}{d\rho^2} + \frac{1}{\rho} \frac{d}{d\rho}\right)^2 \Phi = 0$, and the general solution is reduced to

$$\Phi = A \ln \rho + B \rho^2 \ln \rho + C \rho^2 + D \quad (4d)$$

where A, B, C, D are the arbitrary constant.

Stress component is expressed as:

$$\sigma_\rho = \frac{A}{\rho^2} + B(1 + 2 \ln \rho) + 2C \quad (4e)$$

$$\sigma_\varphi = -\frac{A}{\rho^2} + B(3 + 2 \ln \rho) + 2C \quad (4f)$$

$$\tau_{\rho\varphi} = \tau_{\varphi\rho} = 0 \quad (4g)$$

The normal stress component is only a function of ρ and does not change with φ , and the shear stress component does not exist, so the stress state is symmetrical to any plane passing through the z-axis, that is, symmetrical to the z-axis.

The displacement component under the axisymmetric stress state is described as

$$u_\rho = \frac{1}{E} [-(1 + \mu) \frac{A}{\rho} + 2(1 - \mu) B \rho (\ln \rho - 1) + (1 - 3\mu) B \rho + 2(1 - \mu) C \rho] + I \cos \varphi + K \sin \varphi \quad (4h)$$

$$u_\varphi = \frac{4B\rho\varphi}{E} + H\rho - I \sin \varphi + K \cos \varphi \quad (4i)$$

where A, B, C, H, I, K are all arbitrary constant, and the stress distribution of the subsidy pipe is symmetrical.

Boundary conditions are given by $(\tau_{\rho\varphi})_{\rho=a} = 0$, $(\tau_{\rho\varphi})_{\rho=b} = 0$, $(\sigma_\rho)_{\rho=a} = -q_a$, $(\sigma_\rho)_{\rho=b} = -q_b$.

The boundary conditions are brought into the expression of stress component to obtain:

$$\frac{A}{a^2} + B(1 + 2 \ln a) + 2C = -q_a \quad (4j)$$

$$\frac{A}{b^2} + B(1 + 2 \ln b) + 2C = -q_b \quad (4k)$$

Since the subsidy pipe is multi-piece, it is necessary to investigate the single value condition of the displacement, hence $B = 0$, and the following equation can be obtained.

$$A = \frac{a^2 b^2 (q_b - q_a)}{b^2 - a^2} \quad (4l)$$

$$2C = \frac{q_a a^2 - q_b b^2}{b^2 - a^2} \quad (4m)$$

Incorporating the expression of stress component, the equations are rewritten as:

$$\sigma_\rho = -\frac{\frac{b^2}{\rho^2} - 1}{\frac{b^2}{a^2} - 1} q_a - \frac{1 - \frac{a^2}{\rho^2}}{1 - \frac{a^2}{b^2}} q_b \quad (4n)$$

$$\sigma_\varphi = \frac{\frac{b^2}{\rho^2} + 1}{\frac{b^2}{a^2} - 1} q_a - \frac{1 + \frac{a^2}{\rho^2}}{1 - \frac{a^2}{b^2}} q_b \quad (4o)$$

In this paper, the original outer diameter of the subsidy pipe was slightly larger than the size of the oil pipeline to achieve the purpose of plugging. Therefore, the damaged pipeline has only external pressure on the subsidy pipe, so we obtain the following equations:

$$q_a = 0, \quad \sigma_\rho = -\frac{1 - \frac{a^2}{\rho^2}}{1 - \frac{a^2}{b^2}} q_b, \quad \sigma_\varphi = -\frac{1 + \frac{a^2}{\rho^2}}{1 - \frac{a^2}{b^2}} q_b$$

Obviously, σ_ρ and σ_φ are always compressive stress.

The subsidy tube was subjected to radial external pressure, so radial displacement occurred, and the boundary conditions are expressed as:

$$(\sigma_\rho)_{\rho=a} = \frac{A}{a^2} + 2C = -q_a = 0 \quad (4s)$$

The length of the subsidy pipe in this paper was 3 m, and the axial strain and displacement were assumed to be 0. Therefore, this problem can be regarded as plane strain state. Furthermore, I and K are ignored, and we obtain the following equation:

$$(u_\rho)_{\rho=b} = \frac{1}{E'} \left[-(1 + \mu') \frac{A}{b} + 2(1 - \mu') C b \right] = \Delta l \quad (4t)$$

where $E' = \frac{E}{1 - \mu^2}$, $\mu' = \frac{\mu}{1 - \mu^2}$, and Δl is the difference between the radius of the subsidy pipe in the initial state and that of the damaged pipeline. After calculation, the following equations are described as:

$$A = -2Ca^2, \quad 2C = \frac{E' \Delta l b}{a^2(1 + \mu') + b^2(1 - \mu')}$$

$$\sigma_\rho = \frac{A}{\rho^2} + 2C = 2C \left(1 - \frac{a^2}{\rho^2} \right) \quad (4w)$$

$$\sigma_\varphi = -\frac{A}{\rho^2} + 2C = 2C \left(1 + \frac{a^2}{\rho^2} \right) \quad (4x)$$

Combining the above equations, we get the following expression:

$$q_b = \frac{E' \Delta l b}{a^2(1 + \mu') + b^2(1 - \mu')} \left(\frac{a^2}{b^2} - 1 \right) \quad (4y)$$

$$q_b = \frac{E \Delta l b}{(1 + \mu)[a^2 + (1 - 2\mu)b^2]} \left(\frac{a^2}{b^2} - 1 \right) \quad (4z)$$

Assuming that the radial part of the subsidy pipe was slightly deformed, such deformation could be considered within the elastic range. In this paper, $E = 20$ GPa, $\mu = 0.43$, $b = 63$ mm, $a/b = 0 - 1$, $\Delta l = 0 - 1$ mm, and the functional relationship between external pressure q_b with a/b and Δl is shown in Fig. 21. q_b is the pressure between the subsidy pipe and the damaged pipeline, which is affected by the elastic modulus of the subsidy pipe, and the elastic modulus is a function of temperature, therefore, when the elastic modulus changes with the temperature, q_b also changes.

4.6. The influence of carbon fiber content and temperature on the stiffness

With regard to SMPC, the carbon fiber content and temperature have a significant impact on the structural stiffness. In other words, the higher fiber content and the lower temperature, the higher stiffness. In this paper, carbon fiber fabric was used as the reinforcing phase, and the thickness of each layer was ca. 0.25 mm. The outer and inner diameters of the semicircular hinge were 50 mm and 30 mm, respectively. The SMPC semicircular hinge structure of 0–10 layers was subjected to compression tests at different temperatures, and the corresponding Load-Deflection test curves are shown in Fig. 22. As the test temperature increased, the slope of the Load-Deflection curve gradually decreased, implying that the elastic modulus of SMPC decreased. Especially, when the test temperature was 160 °C, the radial stiffness of many components significantly decreased, owing to the SMPC being already in a rubbery state. The radial stiffness of SMPC with different fiber fabric layers was analyzed by function interpolation, as shown in Fig. 22 (1), and the interpolation function is as follows:

$$y = y_0 + A * \exp(R_0 x) \quad (5)$$

where $y_0 = 8.93$, $A = 66.07$, $R_0 = 0.37$.

It can be concluded from Eq. (5) that with the increase of the carbon fiber content, the corresponding radial stiffness increases exponentially.

4.7. Experimental analysis on radial and axial compression of SMPC pipe

Radial and axial compression tests were performed on the SMPC subsidy pipe wet-wound in the direction of $\pm 45^\circ$ along the axial direction at different temperatures to determine the effect of temperature on the radial and axial stiffness of the subsidy pipe. The subsidy pipe has the shape memory effect, so it is subjected to a radial compression test and heated to make the structure rebound, and then radially compressed and heated again to make the structure rebound to observe the influence of compression times on radial stiffness. Fig. 23(a)(b) shows the mechanical response of radial compression at different temperatures. The higher temperature, the lower the radial stiffness. When the test temperature reached 160 °C, the radial stiffness greatly decreased. However, when the temperature was lower than 100 °C, stiffness did not change significantly. Fig. 23(c)(d) shows the mechanical response under different radial compression times, and the test temperature was 160 °C, owing to the shape memory effect of the subsidy pipe, with the increase in the number of compressions, the radial stiffness showed an exponential decline, which can be referred to Eq. (5), where $y_0 = 3.98$, $A = 153.91$ and $R_0 = -0.56$.

The SMPC subsidy pipe was subjected to axial compression tests at different temperatures. The Load-Displacement curve is shown in Fig. 24(a). As the temperature increased, the axial stiffness gradually decreased. In Fig. 24(b)(c)(d), the strains in the axial direction, fiber direction and transverse direction are shown as a function of time, respectively. With the change of the axial compression displacement, the strains in the axial and fiber directions gradually became smaller, indicating that both axial and fiber directions were under compression. The horizontal strain demonstrates an upward trend, indicating that the subsidy pipe was under tension in the horizontal direction.

In Fig. 25, the SMPC pipe with an outer diameter of 126 mm and a wall thickness in the range of 0.5–2.5 mm was subjected to radial compression tests at different temperatures to observe the effect of wall thickness on stiffness. As shown in the figure, with the increase the tube wall thickness and temperature increase, radial stiffness shows an upward trend.

4.8. On-site construction and installation of subsidy pipes

The molded SMPC subsidy pipe was installed in the appropriate part of the well with the tools and heated to the desired temperature to expand the subsidy pipe and achieve a tight fit with the casing well. The technical parameters of the downhole installation tool are as follows:

Maximum outer diameter: 102 mm; total instrument length: 3,303.5 mm; length of subsidy tube that can be mounted: 0.3 m–2.5 m; instrument weight: 29.5 kg; body material: 17 PH-4 PH stainless steel; maximum pressure resistance: 20 MPa; power supply voltage (heating tube): 220–380 VDC/VAC; rated power (heating tube): 1 kW–3 kW; electrical insulation value: ≥ 400 k Ω ; maximum working temperature: 120 °C.

According to the characteristics of the six-petal cross-sectional shape of the subsidy pipe, an adjustable hexagonal block was arranged on the chuck, and the subsidy pipe was clamped outside the tool. Three hexagonal support plates were arranged inside the subsidy pipe and fixed on the center rod by screws to support the subsidy pipe. The maximum slidable range of the lower fixed plate of the tooling tool was 2.8 m, and the subsidy pipe with a length in the range of 0.3 m–2.5 m was installed. The entire instrument had a very large aspect ratio and was a large flexible rod system. The tool was more seriously deformed due to its weight when it was placed horizontally, so counterweight was not designed. Instead of the weight of the solid center rod, tie rod and tail pressure plate and guide shoes is mainly used as the counterweight. In order to reduce the deformation caused by weight, a structure with two parallel rods, a center rod and a tie rod, was equipped with slender threads and sealing grooves, further enhancing the stability and strength of the system.

The subsidy pipe and the installation tool were assembled on the ground, as shown in Fig. 26(a), and then the overall structure was put into the underground ca. 28.37 m, as shown in Fig. 26(b). After heating for about 260 min, the downhole temperature reached 91.2 °C and the heating continued for ca. 40 min. After the subsidy pipe expanded and deformed, the tooling was smoothly drawn out, as shown in Fig. 26(b). The results showed that the subsidy pipe expanded and was closely attached to the well wall.

5. Conclusion

In this paper, a pipeline repair technology based on SMPC was designed. The SMPC subsidy pipe was prepared by winding carbon fiber wet winding process in the direction of $\pm 45^\circ$ along the axial direction, and the corrosion resistance test of the subsidy pipe was carried out. The results show that the SMPC has excellent corrosion resistance. In addition, the SMPC subsidy tube was subjected to compression tests at different temperatures to observe the relationship between the ambient temperature, the number of compressions and the changes in radial and axial stiffness. The corresponding functions are obtained by function fitting. The higher the temperature, the more of compression times, and the stiffness decreases exponentially. In order to observe the effect of carbon fiber content on stiffness, compression tests were performed on different layers of carbon fiber fabrics by preparing semicircular hinges. It was found that with the increase of carbon fiber content, the radial stiffness of the semicircular structure increased exponentially. Comparing the failure theories of various composite materials and performing corresponding simulation analysis, the thinnest pipe wall satisfying the pressure conditions under different failure theories was determined. Through the mechanical behavior analysis and material performance analysis of SMPC and SMPC-based structures, the relevant factors affecting SMPC and the application prospects of SMPC subsidy pipes for plugging damaged pipelines were further determined.

Declaration of Competing Interest

The authors declare that they have no known competing financial interests or personal relationships that could have appeared to influence the work reported in this paper.

Acknowledgment

This work is supported by the National Natural Science Foundation of China (Grant Nos.11632005).

References

- [1] Liu Z, Lan X, Bian W, Liu L, Li Q, Liu Y, et al. Design, material properties and performances of a smart hinge based on shape memory polymer composite. *Compos B* 2020;193:108056.
- [2] Liu T, Liu L, Miao Yu, Li Q, Zeng C, Lan X, et al. Integrative hinge based on shape memory polymer composite: material, design, properties and application. *Compos Struct* 2018;206:164–76.
- [3] Liu Z, Li Q, Bian W, Lan X, Liu Y, Leng J. Preliminary test and analysis of an ultralight lenticular tube based on shape memory polymer composites. *Compos Struct* 2019;223:110936. <https://doi.org/10.1016/j.compstruct.2019.110936>.
- [4] Zhao H, Lan X, Liu L, Liu Y, Leng J. Design and analysis of shockless smart releasing device based on shape memory polymer composites. *Compos Struct* 2019;223:110958. <https://doi.org/10.1016/j.compstruct.2019.110958>.
- [5] Zhang D, Liu L, Leng J, Liu Y. Ultra-light release device integrated with screen-printed heaters for CubeSat's deployable solar arrays. *Compos Struct* 2020;232:111561. <https://doi.org/10.1016/j.compstruct.2019.111561>.
- [6] Tobushi H, Hashimoto T, Hayashi S, Yamada E. Thermomechanical constitutive modeling in shape memory polymer of polyurethane series. *J Intell Mater Syst Struct* 1997;8(8):711–8.
- [7] Tobushi H, Okumura K, Hayashi S, Ito N. Thermomechanical constitutive model of shape memory polymer. *Mech Mater* 2001;33(10):545–54.
- [8] Liu Y, Gall K, Dunn ML, Greenberg AR, Diani J. Thermomechanics of shape memory polymers: uniaxial experiments and constitutive modeling. *Int J Plast* 2006;22(2):279–313.
- [9] Tan Q, Liu L, Liu Y, Leng J. Thermal mechanical constitutive model of fiber reinforced shape memory polymer composite: based on bridging model. *Composite part A* 2014;64:132–8.
- [10] Noroozi R, Bodaghi M, Jafari H, Zolfagharian A, Fotouhi M. Shape-adaptive metastructures with variable bandgap regions by 4D printing. *Polymers* 2020;12(519):1–21.
- [11] Bodaghi M, Serjouei A, Zolfagharian A, Fotouhi M, Rahman H, Durand D. Reversible energy absorbing meta-sandwiches by FDM 4D printing. *Int J Mech Sci* 2020;173:105451. <https://doi.org/10.1016/j.ijmecsci.2020.105451>.
- [12] Bodaghi M, Noroozi R, Zolfagharian A, Fotouhi M, Norouzi S. 4D printing self-morphing structures. *Materials* 2019;12(1353):1–16.
- [13] Yuan Y, Goodson J, Johnson M. In-situ mechanical and functional behavior of shape memory polymer for sand management application. *SPE*; 2011:143204.
- [14] Ozan C, van der Zee W. Mechanical modeling of shape memory polyurethane foam for application as a sand management solution. *SPE*; 2011:146650.
- [15] Carrejo N, Horner DN, Johnson MH. Shape memory polymer as a sand management alternative to gravel packing. *SPE*; 2011:147101.
- [16] Carrejo N, Horner DN, Johnson MH. The effects of dynamic loading on the sand management and permeability of shape memory polymer and gravel packs for sand management application. *SPE*; 2011:143060.
- [17] Ren Jiaxiang, Gerrard D, Goodson J. Studying the effect of chemical aging on the properties of a shape memory material. *OTC*; 2011:21317.
- [18] Jinlian Hu, Yong Zhu, Huahua Huang. Recent advances in shape-memory polymers: Structures, mechanism, functionality, modeling and applications. *Prog Polym Sci* 2012;37(12):1720–63.
- [19] Ren Jiaxiang, GERRARD D, Duan Ping. Development and characterization of a modified polymeric material for HP/HT downhole sealing applications. *SPE*; 2012:147279.
- [20] Mansour AK, Ezeakacha C, Taleghani AD. Smart lost circulation materials for productive zones. *SPE*; 2017:187099.
- [21] Taleghani AD, Li G, Moayeri M. The use of temperature-triggered polymers to seal cement voids and fractures in wells. *SPE*; 2016:181384.
- [22] Santos L, Taleghani A D, Li G. Smart expandable proppants to achieve sustainable hydraulic fracturing treatments. *SPE*; 2016:181391.
- [23] Osunjaye G, Abdelfattah T. Open hole sand control optimization using shape memory polymer conformable screen with inflow control application. *SPE*; 2017:183947.
- [24] Jinsong Leng, Xie Fang Wu, Xuelian Liu Yanju. Effect of the radiation on the properties of epoxy-based shape memory polymers. *J Intell Mater Syst Struct* 2014;25:1256–63.
- [25] Ramakers-van Dorp Esther, Haenel Thomas, Sturm Frank, Möginger Bernhard, Hausnerova Berenika. On merging DMA and micro indentation to determine local mechanical properties of polymers. *Polym Test* 2018;68:359–64.
- [26] Lahelin M, Aaltio I, Heczko O, Söderberg O, Ge Y, Löfgren B, et al. DMA testing of Ni-Mn-Ga/polymer composites. *Compos A Appl Sci Manuf* 2009;40(2):125–9.

- [27] Camanho PP, Matthews FL. A progressive damage model for mechanically fastened joints in composite laminates. *J Compos Mater* 1999;24(33):2264.
- [28] Hashin Z. Failure Criteria for Unidirectional Fiber Composites. *J Appl Mech* 1980;47:329–34.
- [29] Shen Guanlin, Hu Gengkai, Liu Bin. *Composite Material Mechanics* (2nd ed.). p. 55–61.
- [30] Xia M, Takayanagi H, Kemmochi K. Analysis of multi-layered filament-wound composite pipes under internal pressure. *Compos Struct* 2001;53(4):483–91.
- [31] Bakaiyan H, Hosseini H, Ameri E. Analysis of multi-layered filament-wound composite pipes under combined internal pressure and thermomechanical loading with thermal variations. *Compos Struct* 2009;88(4):532–41.
- [32] Xia M, Kemmochi K, Takayanagi H. Analysis of filament-wound fiber-reinforced sandwich pipe under combined internal pressure and thermomechanical loading. *Compos Struct* 2001;51(3):273–83.
- [33] Bouhafis M, Sereir Z, Chateaneuf A. Probabilistic analysis of the mechanical response of thick composite pipes under internal pressure. *Int J Press Vessels Pip* 2012;95:7–15.
- [34] Chen Jianguo, Liu Liwu, Liu Yanju, Leng Jinsong. Thermoviscoelastic shape memory behavior for epoxy-shape memory polymer. *Smart Mater Struct* 2014;23(5).
- [35] Jianguo Chen. *Viscoelastic constitutive theory of shape memory polymer and its composite*. Harbin Institute of Technology; 2014.
- [36] Zhilun Xu. In: *Elasticity*. China: Higher education press; 2006. p. 61–4.